BRNO UNIVERSITY OF TECHNOLOGY

Faculty of Electrical Engineering
and Communication

Numerica Model of Inhalation

MASTER'S THESIS

Brno, 2017 Selena Milanovic

BRNO UNIVERSITY OF TECHNOLOGY
VYSOKÉ UČENÍ TECHNICKÉ V BRNĚ

FACULTY OF ELECTRICAL ENGINEERING AND COMMUNICATION
FAKULTA ELEKTROTECHNIKY
A KOMUNIKAČNÍCH TECHNOLOGIÍ

DEPARTMENT OF BIOMEDICAL ENGINEERING
ÚSTAV BIOMEDICÍNSKÉHO INŽENÝRSTVÍ

NUMERICAL MODEL OF INHALATION
NUMERICKÝ MODEL DÝCHÁNÍ

MASTER'S THESIS
DIPLOMOVÁ PRÁCE

AUTHOR — **Selena Milanovic**
AUTOR PRÁCE

SUPERVISOR — **Ing. Jiří Sekora**
VEDOUCÍ PRÁCE

BRNO 2017

Brno University of Technology

University of Applied Sciences Technikum Wien

Numerical and experimental study of aerosol particle flow and deposition in a lung simulator

MSc Biomedical Engineering Sciences

Double Degree Program

Author:
Selena Milanovic

Supervisors:
Dr. Jiri Sekora
Mr. Mathias Forjan

19th May 2017

Abstract

The number of animals involved in laboratory testing needs to decrease, according to the latest decrees of the European Union. Furthermore, little is known about the secondary effects of gaseous substances (e.g. deodorants, cleaning sprays) used on a daily basis in every household. Based on these pressing necessities, an analysis of particle transport and deposition has been conducted. The study has been conducted on two levels: on a computational basis (CFD simulations) and on a practical basis. The experimental part of the research is based on the functioning of a lung simulator, the i-Lung. The model can be used as a passive simulator as well as an active one.

Keywords: lung simulator, aerosol, particle flow, particle deposition.

Acknowledgements

It is in a genuine way that I would like to express my gratitude to my mentors.

To Mr Mathias Forjan, I owe the sense of gratification and completion that this thesis gives me. From the very beginning, he welcomed me in his research team and passionately engaged me in the topic. His optimistic and eager attitude towards the outcome of this project repeatedly motivated me to strive for more.
Dr Jiri Sekora I thank for never doubting in my success and giving me the freedom to mold the topics of research following my interests.

Contents

Chapter 1

Introduction

Starting with motivation and aim, the research topic is introduced. Subsequently, an anatomical insight provides information about the human respiratory tract and respiratory volumina. Conducting a study about aerosol particle deposition in airways requires basic concepts to be introduced, as well as production and measurement techniques. Finally, the lung simulator model is described.

1.1 Aim

The aim of the research consists in investigating on particle flow and deposition in a human lung simulator, the i-Lung. In particular, on the one hand the size of aerosols particles that are inhaled by the lung simulator and those that are exhaled will be analyzed; on the other hand the quantity of particles deposited within the module will be identified. A numerical analysis will be conducted, based on the geometry of the i-Lung's airway structure. Subsequently, an experimental validation will be performed and compared to the results of the numerical analysis. Furthermore, differences between literature-based knowledge on particle deposition in human lungs and findings based on the i-Lung model will be highlighted.

1.2 Motivation

"One of the main reasons for developing and adopting the REACH (Registration, Evaluation and Authorization of Chemicals) Regulation was that a large number of substances have been manufactured and placed on the market in Europe for many years, sometimes in very high amounts, and yet there is insufficient information on the hazards that they pose to human health and the environment. There is a need to fill these information gaps to ensure that industry is able to assess hazards and risks of the substances, and to identify and implement the necessary risk management measures in order to protect humans and the environment." [1]
In order to gather the relevant information about hazards and benefits of products on human health it is necessary to perform clinical testing. Very often, it is the case that animals are involved in these kinds of testing. The number of animals involved in these experiments increases year by year. [2]
Therefore, "The new European chemicals policy REACh (Registration, Evaluation and Authorization of Chemicals) has highlighted the urgent need for further progress in the development of alternatives in order to reduce the large projected animal use that will be its consequence." [3]
Aside from the REACH Regulation, restrictions presented in the EU Cosmetic Products Regulation (EC) No 1223/2009 (in act since 2013), are also relevant for decreasing the number of animals involved in clinical testing. Public health is the main focus area of this regulation. Rules about consumption, packaging and labeling of animal products are defined within. Furthermore, The Registration aborts animal testing, specifying bans on:

- Testing: testing of cosmetic products and ingredients on animals;
- Marketing: marketing finished cosmetic products which have have undergone animal testing or which contain ingredients that have been tested on animals. [3, 4]

In order to define a specific amount of animals involved, it is necessary to consider the definition of cosmetics: "A cosmetic product is any substance or preparation intended to be placed in contact with the various external parts of the human body or with the teeth and the mucous membranes of the oral cavity, with a view exclusively or mainly to cleaning them, perfuming them, changing their appearance, and/or correcting body odors, and/or protecting them or keeping them in good condition." [3]

Products such as deodorants or hair-sprays are included in this definition. These are very commonly purchased products, yet apart from their purpose, very little is known about their secondary effects on human health. The aim of this study was therefore to identify the effect of aerosols on the human airways. Models and simulations of the respiratory tract have been developed in order to find answers to these questions. In particular, their flow path and deposition rate was be investigated. The study was carried out on two levels: a numerical analysis and an experimental validation.
With a similar purpose, various simulators have been designed over the past years. Some of them are based on numerical and mathematical analysis, not including ex vivo components. The i-Lung, a lung simulator developed in collaboration of the universities: Brno University of Technology, College of Polytechnics Jihlava and University of Applied Sciences Technikum Wien was the one used for the experimental validation of this study. The collaboration between the aforementioned universities is still ongoing, focusing research on sensors, lung replacement options and specific breathing simulation patterns.

1.2.1 Clinical relevance

"Our respiratory system evolved to have filtration and elimination systems that must be overcome or bypassed in the process of providing local delivery of medications to the lung. Methods for generating aerosols, formulating drugs, and administering medications effectively to the desired site of action constitute the science of aerosol drug delivery." [5] Yet not only the health effects of casual aerosol inhalation have to be considered, but also the consequence of those used for medicinal purposes. Over the last 40 years, major topics in health-related aerosols have been the preparation of suitable test aerosols, the measurement of total deposition, the measurement of regional deposition, the development of the bolus technique, and the study of clearance and retention." [5]
In medicinal purposes, the main focus on aerosols revolves around particle size and chemical properties. Indeed, the size of the particles determines whether and where the particles will deposit. Particles that reach the furthest sites in the respiratory organs range from a size of 0.01 μm to 12 μm. Reasons for this is their diffusion capability and the fact that larger particles are typically deposited in the site of bifurcation of the bronchi. [5]
"For investigations of total deposition in the human respiratory tract a

nontoxic, mono-disperse aerosol is required. The deposition is determined by measuring the particle concentration before and after breathing, requiring a particle of a controllable size." [6] In order to obtain valuable results, experiments on deposition and effect need to be conducted on healthy volunteers. Moreover, a non-toxic aerosol needs to be applied. As an alternative to that, a mechanical lung simulator based on the performance of a primed porcine lung can be used. However, the research topic should not only cover the aspects of influence in healthy lungs. Further relevant information about breathing behavior can be extrapolated by considering pathological breathing during aerosol exposure. The diseases of the human respiratory organ can mainly be categorized in:

- Obstructive diseases;
- Restrictive diseases;
- Vascular diseases;
- Environmental diseases.

The most common types of lung diseases are the obstructive and the restrictive condition. In the United States they constitute the second leading cause of death after cardiac diseases. [7] It is therefore considered to be of relevant importance to focus research projects also on these aspects.

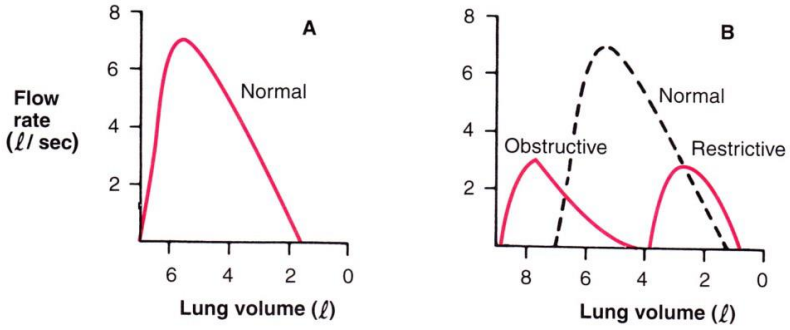

Figure 1.1: A) Normal and (B) obstructive and restrictive exhalation flow curves. Tkaen from [7]

A comparison between flow curves of healthy individuals and unhealthy ones 1.1, reveals the characteristics of a normal airflow. "In obstructive

diseases, such as chronic bronchitis and emphysema, the maximal expiration typically begins and ends at abnormally high lung volumes, and the flow rates are much lower than normal. In addition, the curve may have a scooped-out appearance. By contrast, patients with restrictive disease, such as interstitial fibrosis, operate at low lung volumes. Their flow envelope is flattened compared with a normal curve; but if flow rate is related to lung volume, the flow is seen to be higher than normal." [7] The relationship between volume and flow has to be taken into account, since it influences greatly drug administration in nebulizers. "Inhaled particles follow a complex path through the respiratory tract." [8] Darquenne states the strong interconnection between particle size and lung deposition. Particles ranging 0.4-0.7 μm in size, deposit only minimally in the respiratory tract, as their size permits them to reach further sites in the respiratory tract. This is a common outcome in healthy individuals. Figure 1.2 is a representation of the deposition percentage of particles with respect to their diameter.

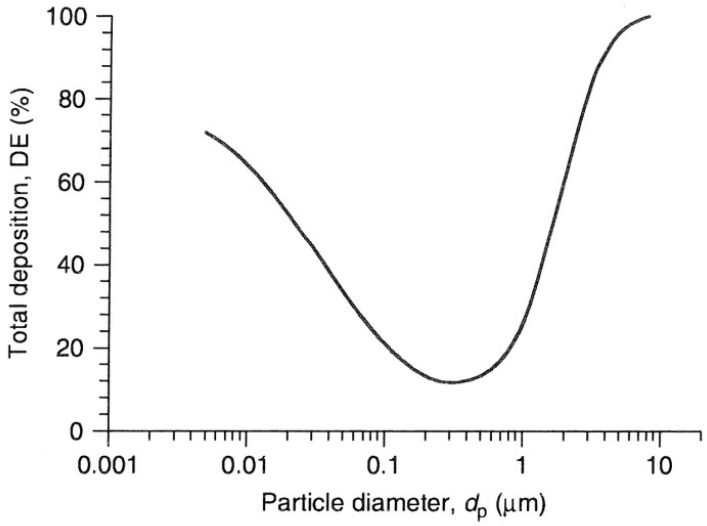

Figure 1.2: Particle diameter curve against the total deposition percentage. Taken from [8]

In unhealthy individuals, the following factors influence the transport and deposition of particles:

- Obstruction of the airways;
- Change of dimensions of the alveoli;
- Pathological breathing patters.

Airway obstructions cause a detour in airflow towards healthy areas of lung tissue. Hence, these specific areas are exposed to a higher load of particle flow. Furthermore, a decreased deposition of particles in the alveolar region is caused. A decrease in airway diameter leads to an increase in stream velocity, leading to an increase in probability of internal impaction. [8]

1.3 Human respiration

1.3.1 Anatomical background

The breathing process begins in the nose and mouth, the inhaled air then follows through the trachea. Subsequently, the trachea divides into two parts named bronchial tubes. Stretching through the lungs, the bronchial tubes divide into smaller branches named bronchioles. The flow stops at the end of the bronchioles, where the alveoli are found. These are tiny balloon-like sacs, and amount to 300 *million* in each individual. Surrounded by a mesh of blood vessels, the alveoli exchange the inhaled air with the blood. The now oxygen rich blood travels to the heart, that pumps it to the rest of the body. Once the cells use the oxygen, carbon dioxide is produced and absorbed into the blood. The carbon dioxide rich blood then flows back towards the lungs where it is ejected during exhalation. [7], [8]
Figure 1.3 shows a representation of the human airways and alveoli. The anatomical structure, function, location and surface area of each component is indicated.

1.3.2 Interpreting respiratory data

In plethysmography "lung volume" indicates the volume of gas contained in the lungs. When conducting tests with the aid of chest radiographs, the referred volume comprehends the volume occupied by the tissue (normal and abnormal) as well. [9] Figure 1.4 shows a volume vs. time spirogram of an inspiratory vital capacity (IVC). Static lung volumes and capacities are defined as sections of the curve.

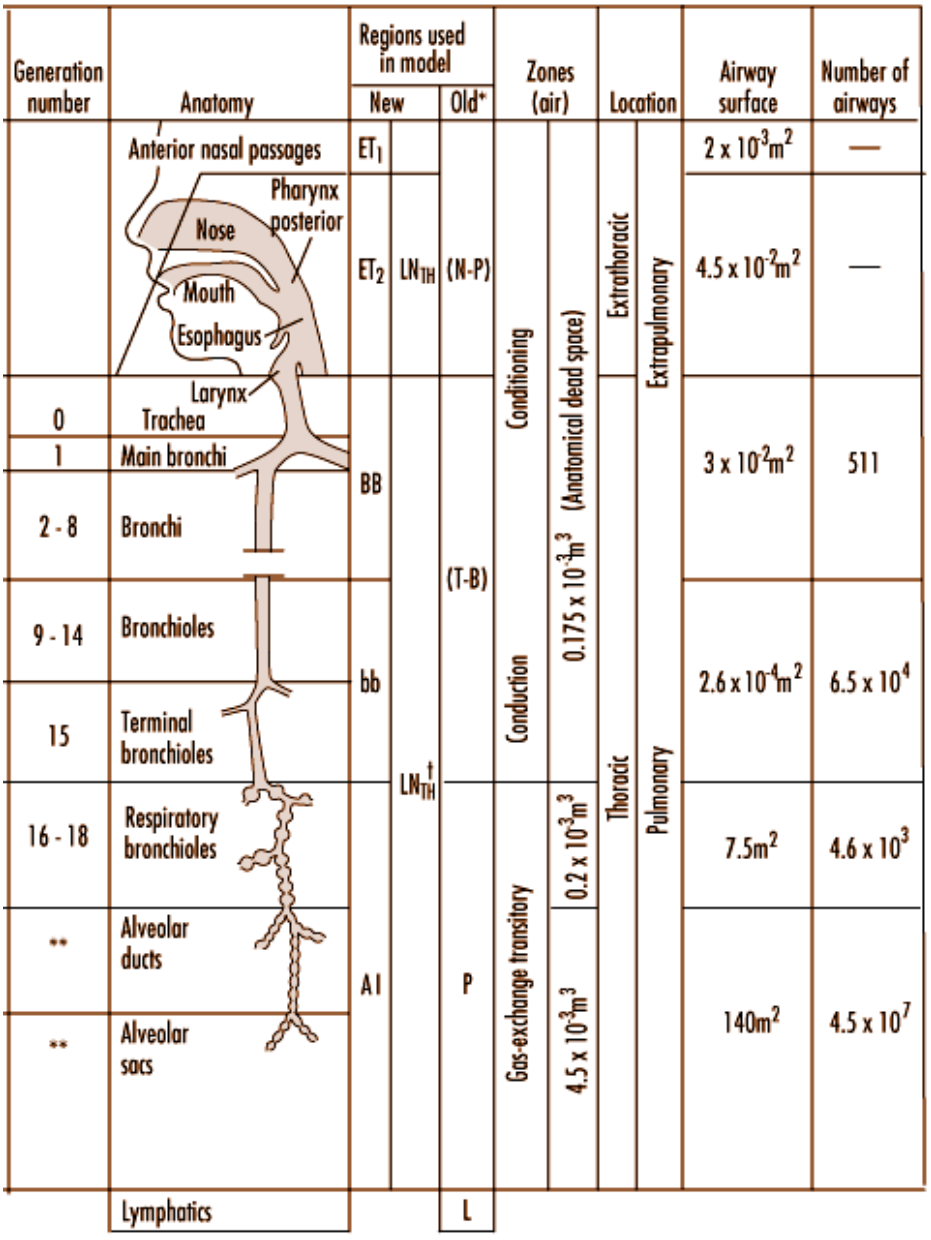

Figure 1.3: Graphical representation of the respiratory system. The generation number, anatomical structure, function, location and surface area are indicated. Adapted picture from [10]

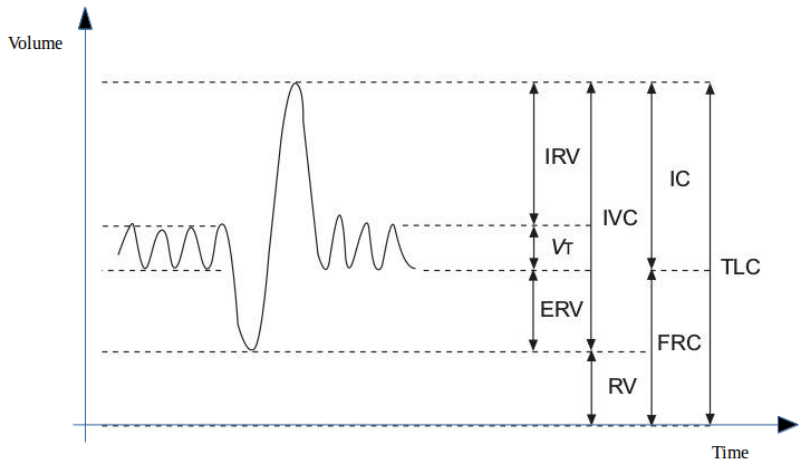

Figure 1.4: Volume vs. time graph presenting the phases and sub-volumina of the respiratory process. Inspiratory reserve volume (IRV); tidal volume (VT); expiratory reserve volume (ERV); residual volume (RV); inspiratory capacity (IC); functional residual capacity. Adapted picture from [9]

- Inspiratory reserve volume (IRV): maximal volume that can be inhaled during tidal breathing (from the end-inspiratory stage). Approximately 3.1 L in men and 0.9 L in women;
- Tidal volume (VT): volume of gas exhaled or inhaled during the respiration. Approximately 0.5 L in both, men and women;
- Expiratory reserve volume (ERV): maximum volume of gas that can be exhaled from the end of expiration. Approximately 1.2 L in men and 0.7 L in women;
- Residual volume (RV): volume of gas present within the lungs at the end of exhalation. Approximately 1.2 L in both, men and women.;
- Inspiratory capacity (IC): maximum volume of gas that can be inhaled. Approximately 3.5 L in men and 2.4 L in women;
- Functional residual capacity (FRC): volume of gas present during tidal breathing (after the end of expiration). Approximately 2.3 L in men and 1.8 Ł in women;

- Total lung capacity (TLC): sum of all lung sub-volumes. Approximately 5.8 L in men and 4.2 L in women. [9]

Other important variables that do not represent a lung sub-volume are:

- Thoracic gas volume (VTG): absolute gas volume at any time and alveolar pressure within the thorax. Approximately 4 L in both, men and women;

- Vital capacity (VC): maximum volume of gas exchanged between a complete inhalation and a slow exhalation. Approximately 4.8 L in men and 3.1 L in women. [9]

1.4 Aerosols

An assembly of solid or liquid particles that are suspended in a gas, for a time long enough to be detected, is named aerosol. The term was coined by August Schamus in 1920, meaning *particle carried by air*. Mainly, aerosols can originate from processes of the following two categories:

1. Natural aerosols: salt particles from sea water, volcano eruptions, desert dust, pollen, smoke particles from forest fires, fog, viruses and bacteria;

2. Industrial aerosols: emissions from heating, transportation vehicles, chemical and mechanical industrial processes. [11]

Particle size and characteristics

One of the most important characteristics of aerosol particles is their size. Assemblies that range from 1 nm up to 100 μm are identified as aerosols. Figure 1.5 presents the complete classification of particles. However, phenomena like charge, velocity and density play a key role. Hence, it is reasonable to confirm that these particles behave according to both, physical and chemical properties. Physical characteristics focus on the friction forces, flow, velocity and acceleration. [12] In an ideal case, the aerosol would be mono-disperse (i.e. all particles are of the same size), however this never occurs. In reality, aerosol is therefore a poly-disperse (i.e. particles of different sizes) assembly. Moreover, physical coagulation

occurs between the particles, which is an additional influence to the performance of the aerosol. [12]

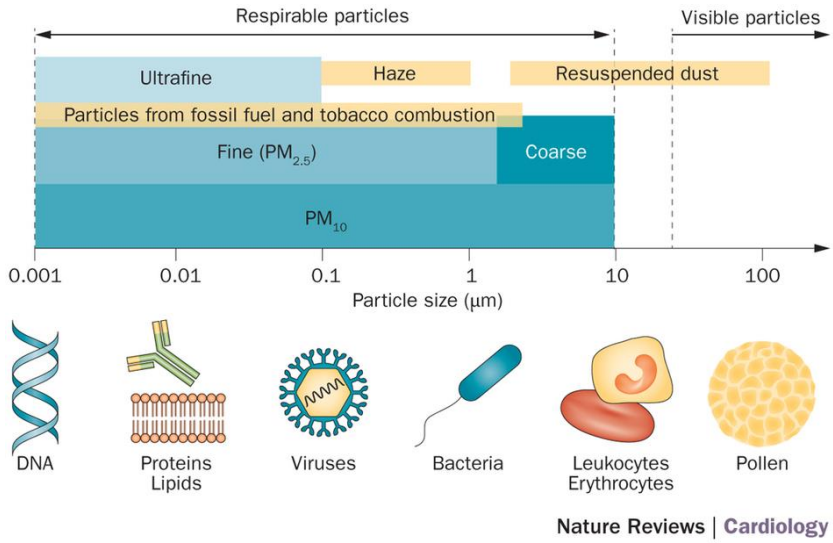

Figure 1.5: Display of Particulate Matter (PM) classification depending on diameter. Taken from [12]

1.4.1 Aerosol production

Depending on the necessities of the research, mainly two types of aerosols can be produced: mono-disperse and poly-disperse. It is necessary to underline that the production of mono-disperse particles is an idealization, as the particles will still have small differences in diameter compared to each other. Nevertheless, this differences are negligible and the gas is still denoted as *mono-disperse*. Typically, mono-disperse aerosols are used for the calibration process of devices measuring particle size. Poly-disperse aerosols instead, are applied during the actual test performance. Hence, an essential characteristic of an aerosol generator is its reliability on producing the specified aerosols. [13]
Various types of generators have been designed, distinguished by the particle type they generate. The main differentiation during production lies in the particle state, which can be either solid or liquid. Mainly, the distinction consists in a process that either condensates of disintegrates larger structures. [14]

1.4.2 Aerosol measurement

Aerosols measurements can be completed with various techniques. Easier methods are the ones that imply the collection on a filter that will be analyzed in a subsequent process, more complex ones include complex measurement instruments. Therefore, there is mainly a distinction between two different categories:

- Collection of aerosols (e.g.filter) and subsequent analysis: economical, time consuming, allow quantitative and qualitative aerosol measurements;
- On the spot detection sensors: expensive, fast results, provide information about size distribution. [6]

Choosing the measurement technique is therefore an important aspect, and has to be a decision that considers all the aspect of the study to be performed. Both techniques can therefore be suitable, depending on the needs. [6] The most commonly used approach for measuring the mass of particles, consists of a vibrating surface on which the particles adhere and subsequently the change of resonance frequency can be measured by electrical charge. However, the limitations of this technique comprise that it is suitable only for small and sticky particles. Another popular measurement technique consists in associating the light scattered by each particle and associating its intensity to a specific diameter. [6]

Equivalent diameter

Equivalent diameters have been introduced since the geometric diameter of the particles is not perfectly shaped. They refer to a parameter that is the measurable index of the particle. [6] The assumption consists in assuming a perfectly spherical shape and assigning its properties to the particle itself.

- **Diffusion diameter:** The size of particles in the sub-micrometer area are described with a diameter that is the one of a standard-density spherical particle that has the same diffusion rate of the one being measured;
- **Aerodynamic diameter:** The aerodynamic diameter corresponds to the one of a particle that has the same gravitational settling velocity

as the one being measured. The introduction of this term is particularly interesting for describing the particle inertia inside the respiratory tract;

- **Optical diameter:** The optical diameter is of use when studying optical properties of particles (e.g. light scattering). The total amount of scattered light is given by a complex function influenced by size, shape and other parameters such as wavelength or scattering angle;

- **Electrical mobility diameter:** The electrical mobility diameter describes the particle behavior in an induced electrical motion. Hence, the path of the moving particle is predictable;

- **Sauter mean diameter:** This droplet diameter defines the surface-to-volume-ratio with respect to all the droplets in the spray distribution.

- **Projected area diameter:** This approximation method consists in measuring the area of the particle and associating to it a circle with the same diameter. Biases of this method include the errors caused by particles shrinking in size or mass. [6]

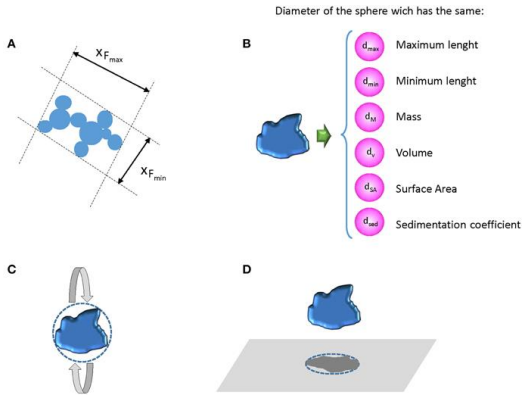

Figure 1.6: A) Possible external dimensions of an irregular aggregate; (B) different diameter expressions when an irregular particle is approximate to a sphere, (C) diameter of a sphere that has the same inertia of rotation, and (D) diameter of the circle causing the same electro-shadow area.Taken from [6]

1.5 Deposition of particles in human airways

After air has been inhaled, the channels through which it passes narrow as the alveoli are closer. This causes the flow to reduce in speed, a factor that increases the deposit time of the particles. The main deposition mechanisms are: impaction, settling, diffusion and interception. [15, 13] The airways of the head and lungs have supplementary muco-ciliary transport, which enables the deposited particles to be removed within several hours or days. As studies show, particles ranging 1-10 μm deposit in the airways of the head; particles ranging 0.01-1 μm remain trapped in the tracheoidal region and particles of 0.01 μm or smaller reach the alveolar cavities. [16] Furthermore, the gas supply in the lung lobes is strongly influenced by the geometry of the bronchioli. Figure 1.8

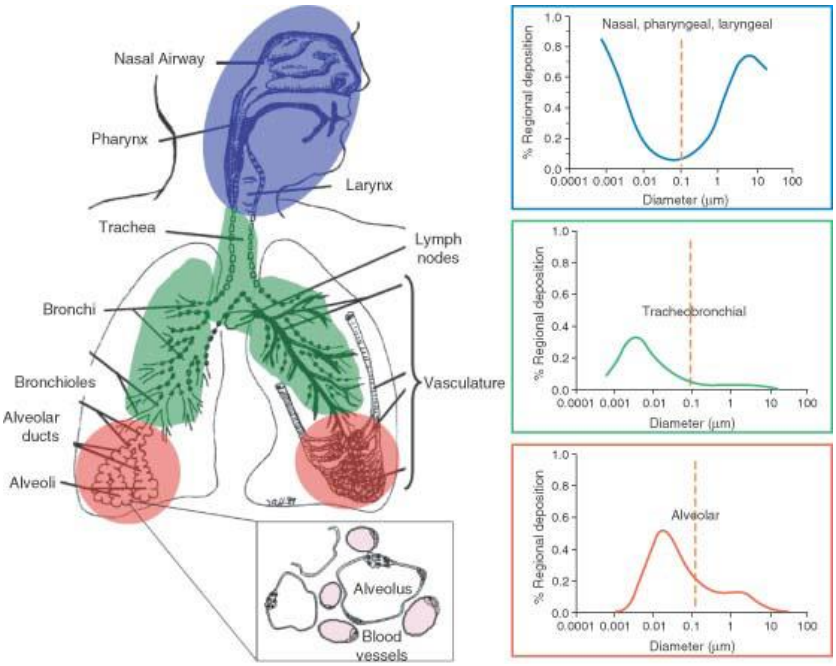

Figure 1.7: Particle deposition in airways. Particles with diameter 1-10 μm deposit in head airways (blue); particles of 0.01-1 μm diameter remain trapped in the tracheoidal region (green) and particles of diameter 0.01 μm remain in the alveoli (red). Taken from [16]

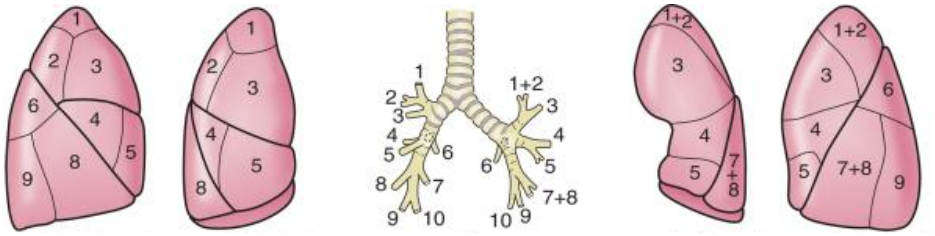

Figure 1.8: Airway connection of bronchioli to lung sections. The perfusion quantity is strongly influenced by this geometrical supply that specifically targets regions of the lung lobes. Adapted picture from [17]

1.5.1 Stokes Law

Particle inertia is a great source of error, hence particles with greater diameters are more problematic. Smaller particles instead follow the stream with negligible inertia, which leads to a nearly perfect sampling. This phenomenon is described by Stokes law as follows:

$$F_D = 3\pi\eta V d \tag{1.1}$$

Where F_D is the total drag force (i.e. air resistance against the passing particle) on a spherical particle with diameter d, moving with a velocity V through a fluid whose viscosity is η. The concept of Stokes friction force (F_{slip} or F_{drag}) is introduced in order to determine the velocity of an aerosol particle. Hence, within the range of validity of the law that corresponds to a laminar flow (i.e. $Re < 0.1$), the slip correlation factor is given by 24/Re. It is also known as the Cunningham correlation factor C_c and is essential for the description pf particles whose size is below 1 μm. [13]

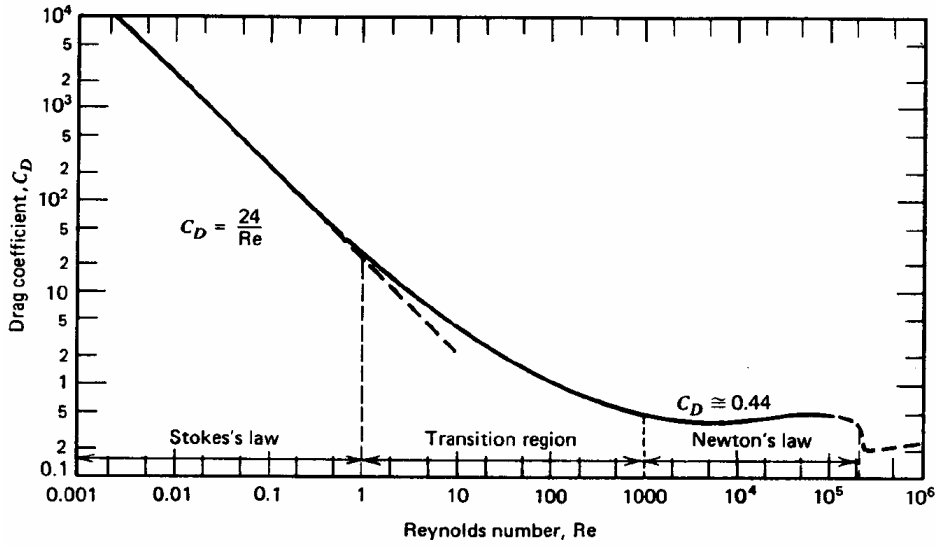

Figure 1.9: Drag coefficient F_d, against the Reynolds number Re for spheres. Taken from [13]

1.5.2 Reynolds number

Since aerosol is a gas mixture of particles suspended in a gas medium, the motion of the particles largely depends on the suspension medium. Particles with a diameter smaller than 1.0 μm are influenced by the motion of each gas molecule, hence for the understanding of their flow basic knowledge of the kinetic gas theory is necessary. Small particles are therefore considered to be in a free molecular regime. On the other hand, large particles can be regarded as in a continuous gas-like fluid and are therefore stated to be in the continuum regime. Understanding of the gas flow pattern is essential for clarifying what influences the measurement, within the measuring device itself as well as at the sensors. In most cases the aerosols follow the path of the gaseous medium, however sometimes anomalies arise due to external forces. The Reynolds number Re is introduced in order to evaluate the level of smoothness or turbulence of the flow pattern. It is defined by the ration of internal force and the friction force medium it is flowing through. [13]

$$Re = \frac{V d \rho_g}{\eta} = \frac{V d_p}{\nu} \tag{1.2}$$

Where V is the speed of the medium, η is the dynamic gas velocity, ν is the kinematic viscosity and d_p is the diameter of the particle. [13]
With elevated friction forces, the Reynolds number is low (<2000). This results in a laminar flow (i.e. streamlines continue following the same direction without looping back on themselves). Instead, when the inertial forces are higher, the Reynolds number is also high (>4000) and the flow is turbulent (i.e. streamlines loop back on themselves and change the flow direction abruptly). [13]

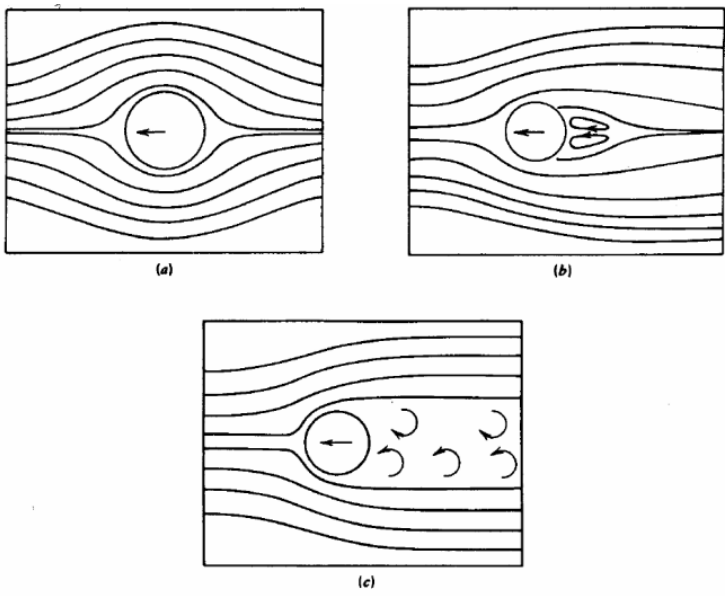

Figure 1.10: Flow around a sphere, (a) laminar flow, (b) turbulent flow with lower Reynolds number of gas, (c) turbulent flow with higher Reynolds number. Taken from [13]

1.6 State of the art research on particle flow and deposition in airways

1.6.1 CT based geometry models

Researchers have established that the most reliable studies on particle flow and deposition in human airways are based on CT geometry of the respiratory ducts. A benefit for using CT-based geometry is the inclusion of all five lung lobes. In simplified models of CFD (computational fluid dynamic) studies, symmetric lung geometries are introduced that do not account for the five distinct lobes of the lungs and therefore cannot conclude a relationship between particle transport and lobar ventilation. It was shown that particle deposition is greater in the lower lobes of the lung. Fewer particles flow through the upper lobes, with an exception of the left-upper lobe which has an elevated quote of particle ventilation of size 2.5 μm and 5 μm. A possible justification for this phenomenon is the fact that these particles present a lower Stokes number, and therefore do not undergo radical deposition in the curved bronchi and bifurcations. Instead, particles of 10, 20 and 30 μm are less free to move throughout the left lung. More generally, there is a marked asymmetry between left and right lung. The left lung receives a greater proportion of particles, in spite of a greater ventilation of the right lung. Indeed, 90% of the particles at total lung capacity (TLC) were situated in the left lung. [18] Three different features can be identified in the human airway: the glottal constriction, cross sectional area of the left main bronchi (LMB) and the location of the carina with respect to the glottis and the upper trachea. Constrictions at the glottis and at the LMB cause a high-speed flow through the trachea and LMB. In the core region of the laryngeal jet, the particles are highly concentrated. While traveling past the glottis and through the trachea, they shift to the peripheral region of the jet, where they are mixed with the residual air found within the duct. The elevated turbulent kinetic energy (TKE) is associated to this process. The Stokes number of the particles determines the dispersion degree. Indeed, particles with a large Strokes number are less uniformly distributed compared to the ones with lower values, and they are also less affected by flow disturbances. Hence, the asymmetry of the particle distribution is further enhanced by the tendency of particles with high Stokes number to remain in the same position.

Studies of this particular behavior tend to agree with the concepts proposed by Crowe et. al (1985, 1988): the Stokes number (i.e. the ratio of the particle's aerodynamic response time over the transit time for large turbulent eddies) is the key for understanding dispersion in flow structures. Indeed, for Stk $\ll$ 1: particles follow the motion of the fluid, whereas for Stk $\gg$ 1: particles become unaffected by changes in velocity fluctuations. Stokes number and particle distribution in the glottis are identified as the main reasons for an asymmetric particle distribution in the lungs. Therefore, the amount and nature of vortices in the glottis is associated to the particle release time during inhalation. [18] This concepts serve to conclude that in the absence of a physiologically-realistic airway model and a large eddy simulation (i.e. considering turbulent fluctuations) the accuracy of the model is greatly affected to a degree that does no longer account for the asymmetric behavior of the flow.

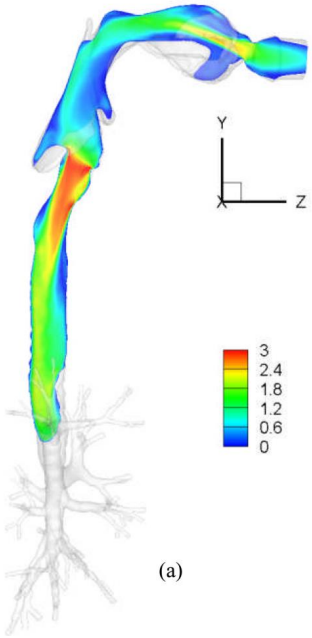

Figure 1.11: Contours of mean particle flow velocity in a CT based airway model. Highest velocity (red) is reached at the trachea inlet where a narrowing of the airway occurs. Adapted picture from [18]

Size (µm)	U/L Right	+/−	U/L Left	+/−
30	0.21	0.08	0.52	0.37
20	0.41	0.28	0.42	0.34
10	0.40	0.09	0.38	0.07
5	0.46	0.09	0.41	0.07
2.5	0.47	0.12	0.45	0.08

Figure 1.12: Deposition ratio between upper (U) to lower lobes (L) U/L, for the right and left lungs. Taken from [18]

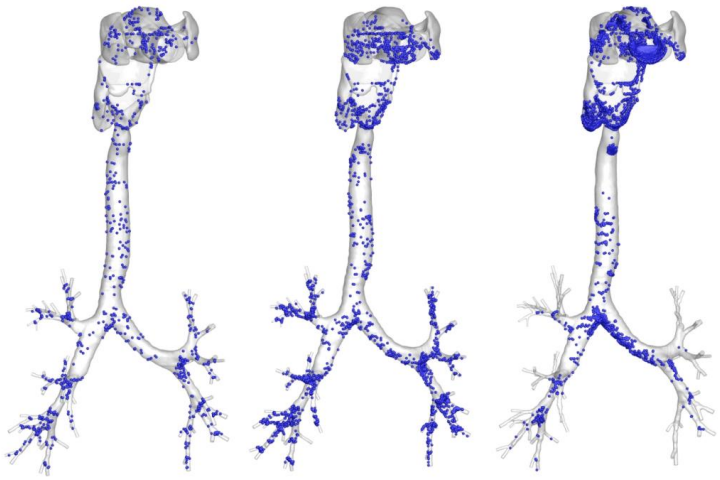

Figure 1.13: Particles with 2.5 μm diameter deposit mainly at the bifurcations of the bronchioli (left); particles with 10 μm diameter deposit in the airways of the mouth and the first stage branching of the bronchi (center); particles qith 30 μm diameter deposit in the pharynx, larynx and trachea branching (right).Taken from [18]

1.6.2 Influence of mucus lining on particle flow and deposition

The internal lining of the airway ducts also has a great influence on the particle flow ad deposition. Researchers have investigated on the specific influence of the mucus lining. A feature of the mucus layer is that it changes generation after generation, hence the study recreated a multi layer mucus structure. Exploiting the Lagrangian particle tracking method, particle transport and deposition were analyzed. The Larangian Discrete Phase (DPM) model has proven to be the most suitable for considering air as a continuum phase and particle as a disperse phase. The model considers the interaction with the continuum phase. The particle release is characterized by different injection properties. The boundary conditions are defined as the velocity at the inlet and the pressure at the outlet. Furthermore, the boundary condition of the internal walls is a trapping one. This means that particles colliding with the internal surface remain trapped in that position.[19]
Particle size of $1\mu m$, $5\mu m$ and $10\mu m$ were considered during the simulation. Following the theoretical knowledge, large particles tend to remain trapped in the upper airways. Indeed, out of the 1016 particles of 10 mum size that were released, 428 remained captured in the first generation whilst the rest were exhaled. Out of all the deposited particles, 159 were deposited during the first 100 iterations which furthermore confirms the theory. For smaller particles, such as $5\mu m$ and $1\mu m$ a similar scenario appears, yet overall less particles remain trapped. [19] In general, studies affirm that the all the particles inhaled during respiration follow the air streamline. However, at points of bifurcation and curvatures the particles tend to deposit on the surface. By adding the mucus layer the geometry of the airways drastically changes, in particular the inlet surface is reduced. This change results in an alteration of the deposition pattern. The change can primarily be noticed in the discrepancy of the data between particles of 10 μm and the smaller ones. It appears that particles that are minor in size deposit only after the second generation and in branches that are smaller in size. Furthermore, the presence of mucus drastically reduces the deposition quantity of the particles. [19]

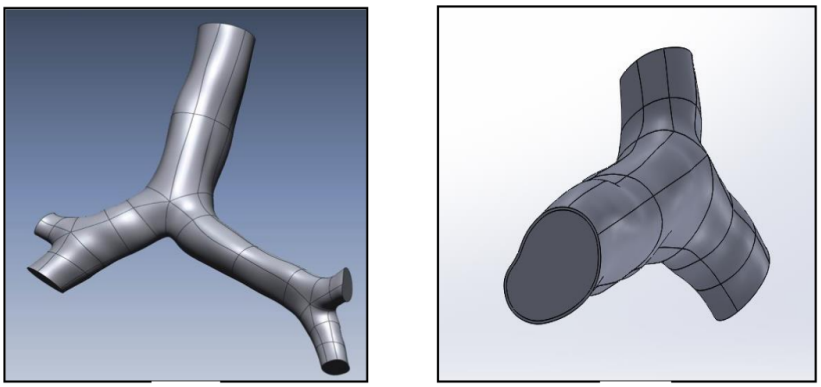

Figure 1.14: 3D geometry of trachea and bronchi. On the left the smooth wall surface model, on the right the multi layered mucus representation. A deformation of the cross sectional area given by the mucus lining is visible. Taken from [19]

1.7 i-Lung respiration simulator

The need for lung simulators arises primarily because of the necessity for testing mechanical respirators. Artificial respirators are used in in various scenarios, such as surgeries or emergencies.

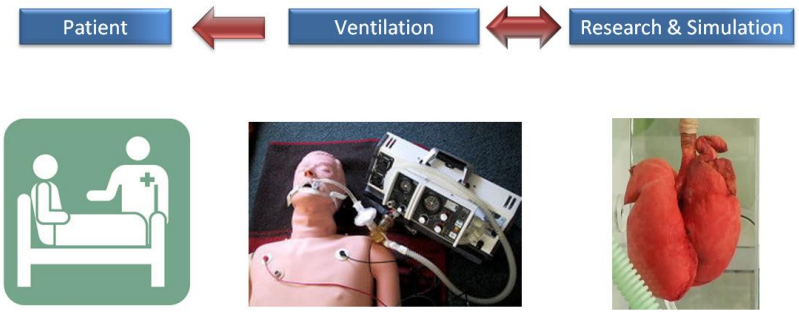

Figure 1.15: Necessity for lung simulators for testing of ventilators that maintain vital parameters of patients unable to breathe (e.g. surgery, emergency). Taken from [6]

1.7.1 i-Lung working principle

In the past years, several models of lung simulators have been developed mainly for educational purposes. The currently existing models can be classified into two main categories: active and passive simulators. Active simulators are designed to simulate active breathing lungs while passive simulators are intended to be ventilated by an external source. However, both models inflate a latex bag (i.e. lung equivalent) which performs adequately for simple study purposes. The development of the used lung simulator, the i-Lung, is described by Wurm [20]. The simulator is a suitable choice for usage such as teaching and testing. It is possible to combine the simulator with an aerosol generation machine in order to obtain more sophisticated and realistic models. Moreover, it is possible to choose between different breathing patterns, one physiological and five pathological.

The emulation of the thoracic chamber in the i-Lung is mimicked by a transparent box (d) made of PMMA (polymethylmethacrylate). In order to minimize negative pressure losses, the chamber must be sealed. The negative pressure is generated by an external vacuum pump (a), simulating the adhesion of pleural membranes. A bellow system is used in order to emulate the changes in intrapulmonary pressure. A ball screw is connected to the motor through a threaded connection and to the lower section of the bellow. Hence, an upward and downward movement is achieved by the rotation of the ball screw through the motor. During the compression phase of the bellows the pressure changes and induces an upward movement; on the other hand, an extension of the bellows causes a downward movement. [21] Figure 1.16 shows the detailed schematics of the i-Lung functioning, whereas Figure 1.17 shows the actual lung module.

The latex bag of the i-Lung can also substituted with a primed porcine lung. Figure 1.18a and Figure 1.18b show a sequence of photographs representing inhalation and exhalation performed by the i-Lung based on a biological lung.

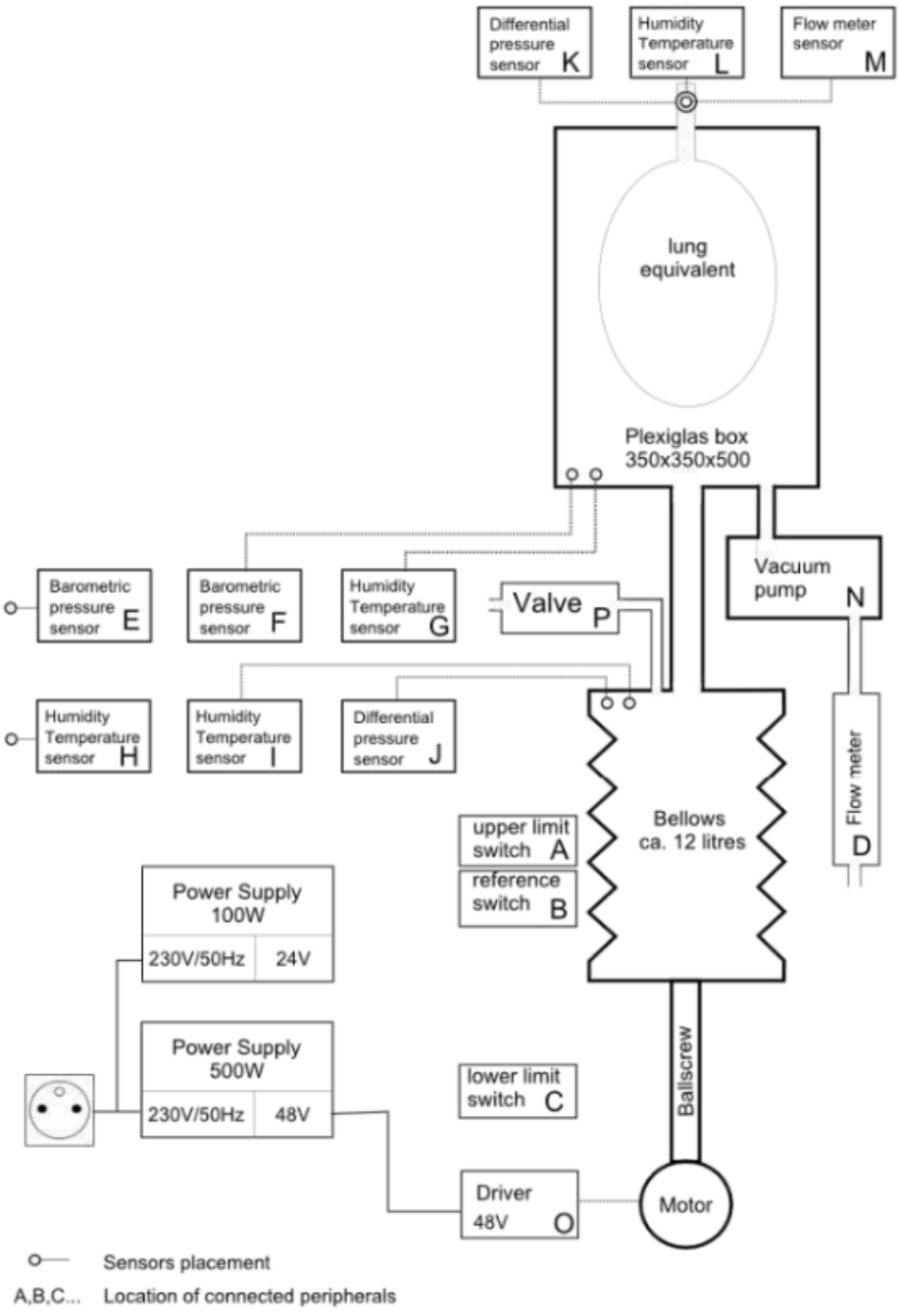

Figure 1.16: Schematics of the i-Lung components and working principle. Adapted picture from [21]

Figure 1.17: iLung model where (a) interchangeable lung equivalent, (b) diaphragm membrane cylinder, (c) DC motor, (d) PMMA chamber and (e) dispensable connection tube for in- and exhalation

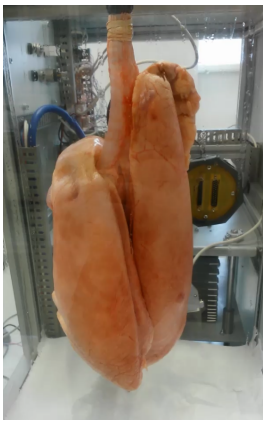

(a) deflated porcine lung

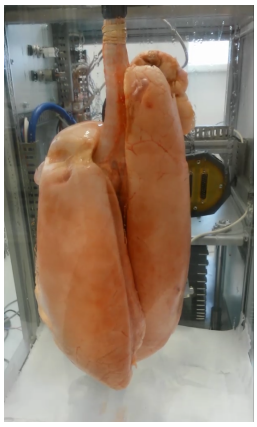

(b) inflated porcine lung.

Figure 1.18: Primed porcine lung during deflation (a) and inflation (b), alimented by the i-Lung machine.

1.7.2 i-Lung validation

With the aim of validating the performance of the lung simulator machine, a set of spirometry tests was conducted. A group of volunteers was gathered and spirometry measurements of their tidal breathing patterns were conducted. The group was sub-dived into two equal-in-number groups, one of individuals with smoking habits and others with no smoking habits. The distribution of male and female participants was equal, and the age group was defined as 22 - 30 years.
The tidal breathing of the individuals was measured 2 times per individual and subsequently the data was averaged. It was therefore possible to obtain a regime of volume characteristic for each subgroup and in the end compare it with the performance of the i-Lung machine. The best visualization of the comparison is provided by the plot of the flow curve for each category: smokers, non-smokers and i-Lung. The graph provides clear evidence of its reliability, highlighting a significant similarity to the flow curve of non-smoking individuals. Hence, it was concluded that the model is suitable for a reliable comparison to the results provided by the computer simulations. [22]

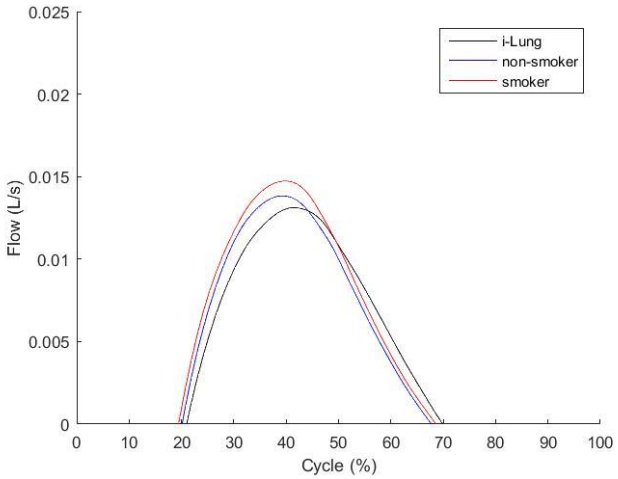

Figure 1.19: Normalized flow curve of each category of individuals. The strong similarity between the non-smokers and the i-Lung is highlighted and the machine is therefore a suitable tool for the validation of the simulation's results. Taken from [22]

Chapter 2

Materials and Methods

The study about particle flow and deposition was conducted with two approaches: numerical simulation and experimental validation. At first, realistic modeling of human airways was attempted. Subsequently, numerical models of the i-Lung's airways were realized and a CFD analysis of aerosol flow was conducted. Validation of the results achieved through simulations was obtained by realizing a suitable experimental setup.

2.1 Numerical analysis

The design of a suitable model representing the human airways presents challenges of different nature. Firstly, the complexity of the geometry of the model itself has an extensive impact on the deposition of the particles. Secondly the smoothness of the internal walls also contributes to the outcome of the analysis. See section 1.6.
Three models will be presented in this study:

- Realistic human airway model: dimensions are based on actual human airways described in literature;
- i-Lung based trachea and bronchi model: dimensions are based on the airway ducts of the lung simulator.
- i-Lung based pharynx model: for the experimental validation, a connector tube had to be designed to connect the i-Lung to an aerosol generator and a spectrometer. Hence, a "pharynx" was designed with

Inventor and 3D printed. A flow analysis was also conducted in order to observe the behavior of the flow before entering the i-Lung.

Both models are products of a balance between realism and feasibility. Mainly, the dimensioning is realistic whilst the surface linings are simplified greatly. Each simulation is based on a design with Autodesk Inventor 2016, followed by a computational fluid dynamic (CFD) analysis with CFD Autodesk 2016. The primary aim of the flow analysis is to identify the path of the particles and their interaction with the internal walls of the airways. The analysis is based on Large-scale Eddies (LE) simulations and Navier-Stokes equations for incompressible flow. LE energy containing turbulent eddies are resolved and small-scale eddies are parametrized with a sub-grid scale model.

$$\frac{\partial u_i}{\partial x_i} = 0 \tag{2.1}$$

$$\frac{\partial u_i}{\partial t} + u_i \frac{\partial u_i}{\partial x_i} = -\frac{1}{\rho}\frac{\partial p}{\partial x_i} + (\nu + \nu_T)\frac{\partial^2 u_i}{\partial x_j \partial x_j} \tag{2.2}$$

where u_i is the filtered velocity component in the i direction, p is the filtered pressure, ρ is the fluid density, ν is the kinematic viscosity, and ν_T is the SGS eddy viscosity. The properties of the fluid are $\rho = 1.2$ kg/m^3 and $\nu =$ 1.7x 10^{-5}m/s at ambient conditions. [18]

2.1.1 Realistic human airway model

The anatomical model of the trachea, bronchi and bronchiole was introduced with the aim of analyzing the particle distribution and flow within the tract. The primary interest lies in identifying the behavior of the flow in critical zones such as the branching of airways and the change in cross sectional area. The airway model has been created with Autodesk Inventor, connecting cylinders of different diameters. The composition (i.e. size and angles) is based on the anatomical structure of human airways. [23] The edges where connection occurs have been smoothed in order to mimic the real-life structure. In order to further minimize the complexity of the analysis, only the right bronchi has been designed with its correspondent bronchioli. The reason for choosing the right bronchi is the fact that it is the one that mostly influences the respiratory volume. Indeed, due to the difference in branching angle from the trachea, diameter

and length, the right bronchi provides the right lung with more airflow. A consequence of this phenomenon is the larger size of the right lung compared to the left lung lobe.
A requirement for a finite element CFD analysis, is the meshing of the 3D body. In order to ensure reliability of the simulation a meshing size of 0.1 has been selected. Indeed, a smaller meshing size ensures higher precision of the outcome. This is particularly valid for models such as this, where small changes in geometry have a large effect on the particle's path. The shape of the meshing elements is tetrahedral, characteristic for 3D objects with irregular and un-symmetric geometries.
Despite the simplifications of the model, the computational time of meshing consists of several hours, exceeding therefore an acceptable limit for executing a continuous flow dynamics analysis. In order to overcome the issue of very elevated computational resources, the scientific community is currently conducting research about particle deposition basing it on CT geometrical models. See section 1.6.

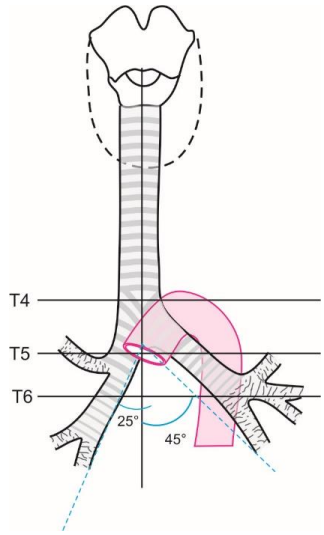

Figure 2.1: Schematic representation of the human airways. The principal regions are identified: Trachea (T4); left bronchi (T5); right bronchi (T6). The angle of inclination for each bronchi is indicated: left (25 ° ; right (45 °). Taken from [24]

Section name	Section symbol	Dimension
Trachea diameter	T4	23 mm
Left bronchioli diameter	T5	13 mm
Right bronchioli diameter	T6	15 mm
Angle between O,T5	(O,T5)	25 °
Angle between O,T6	(O,T6)	45 °
Trachea length	T4T3	150 mm
Larynx length	T3T2	25 mm

Table 2.1: Dimensioning og the airway CAD model used for the flow analysis.

2.1.2 i-Lung based trachea and bronchi model

Based on the dimensions of the i-Lung's airway structure, a model consisting of the larynx, trachea and the two bronchi was designed using Autodesk Inventor 2016. The modeled parts have the same dimensions as its anatomical equivalent, referred to in Table 2.1. The entire structure is hollow in order for the CFD analyzer to distinguish between surface walls and airflow. Indeed, after importing the solid model from Inventor to CFD, it is necessary to select all the volumes composing the model and mark them as solid parts. In the preferences, the solid parts were identified as completely non deformable. This is justified by the fact that the airflow exerts a force on the rigid walls, that is negligible in comparison to the material's deformation factors. The hollow volume of the structure is also selected and identified as the moldable volume. Hence, at the end of the volume selection process the model to be analyzed is composed of two volume types: solid and liquid.
The boundary conditions are identified through pressure and flow. The inlet surface of the model is selected and an inlet flow of 6 $L\,\mathrm{min}$ is applied. The outlet surface area is selected and assigned a 0 Pa pressure. The choice of flow and pressure as boundary conditions of inlet and outlet is a convention used in CFD analysis with Autodesk.

2.1.3 i-Lung based pharynx model

A model of the pharynx was designed in order to connect the i-Lung with the aerosol inlet as well as the spectrometer identifying the particles flowing. In particular, the inlet of the pharynx model represents the connection with the tube delivering the aerosol flow, whilst the outlet of the pharynx mode

is connected with the trachea of the i-Lung. Hence, the real life human anatomy of pharynx and trachea is mimicked.
Furthermore, being a particle measurement assessment necessary, the newly designed inhalation duct (i.e. pharynx model) had to have an additional outlet hole, through which a tube will connect it to the spectrometer.
Similarly to the trachea and bronchi model, the pharynx model was created with Autodesk Inventor 2016 and subsequently imported in CFD in order to conduct a flow analysis. The aim of the analysis was identifying the path of the aerosol flow, the interaction with the internal surface walls and the speed of flow. In analogy to the model described in 2.1.2, the pharynx model has a hollow geometry. Thus, the shell of the model was assigned the characteristics of a solid part, whilst the inner hollow volume was a liquid and moldable volume. This selection process was performed as the model was imported in CFD. Subsequently, the boundary conditions were defined. As characteristic for flow analysis in vessels, the boundary conditions are represented by flow at the inlet and pressure at the outlet. Indeed, the inlet cross sectional area has been marked with an inlet flow of 6 L/min and the outlet cross sectional area has been assigned a pressure of 0 Pa. The choice is justified by the fact that the inlet corresponds to the connection with the aerosol delivery tube, whilst the outlet corresponds to the connection with the i-Lung's trachea.

3D printing of the connector duct

After studying the model with Autodesk software for the design itself and the computational fluid dynamics analysis, the model was printed using the 3D printer Ultimaker 2. Through the software Cura, the model was converted from an *.ipt* solid Inventor file to a *.stl* file and modified in order to fit the printer's needs. In particular, small changes in geometry had to be made in order to accommodate the size of the printer's nozzle. The material used for printing was bio-plastics, in order to guarantee the precision and smoothness of the bio-compatibility and a smooth internal structure. To further enhance the quality of the print, the highest quality level for the print was selected. Additionally, in order to optimize the printing a support structure was printed around it as well as within the pipe. It is important to choose a coarse and low infill density in order to avoid un-smooth surfaces within. Furthermore, a light and coarse internal support structure is preferred as it is easy to remove and less likely to

damage the internal structure of the model. All friction within the pipe must be minimized in order to guarantee a constant flow of gas. The time needed to print the entire object consisted in approximately 11 *hours*, due to the demanded high quality of the grid.

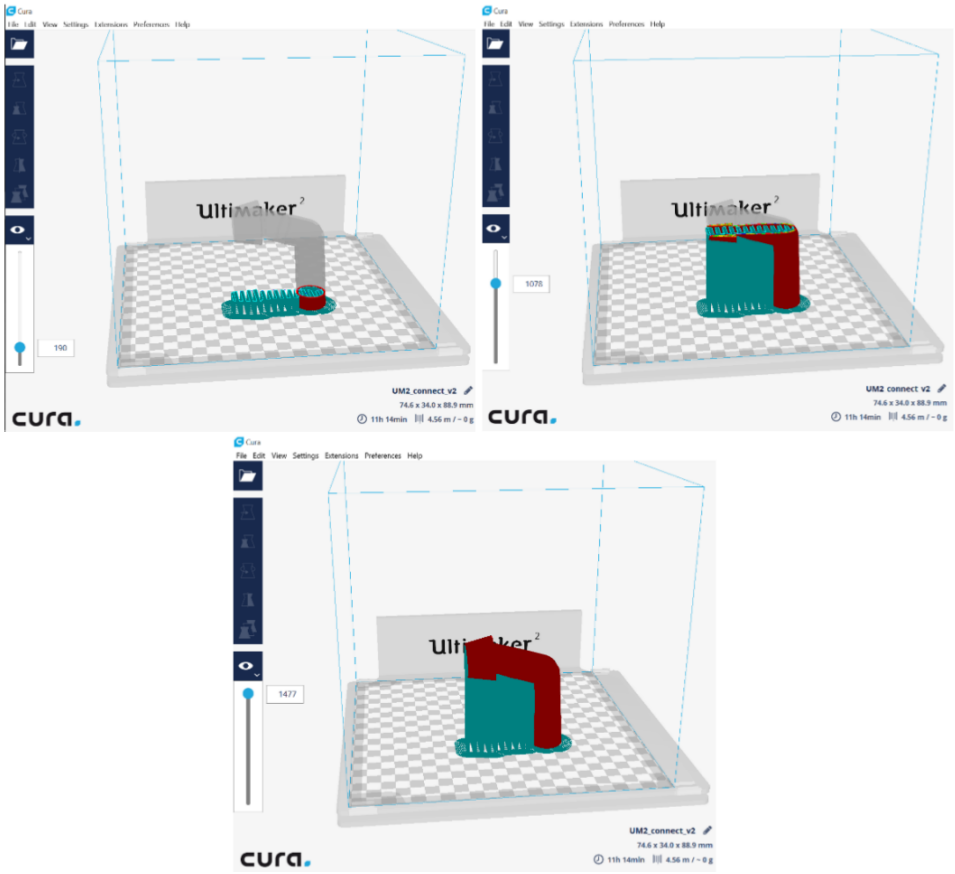

Figure 2.2: A support structure (blue) was designed additionally in order to provide stability during the printing of the main body (red). Three stages of printing are shown: (a) 190 slices, (b) 1076 slices and (c) complete model.

2.2 Experimental validation

2.2.1 Experimental setup

The setup in Figure 2.3 was designed in order to identify and quantify the aerosol particles that flow in and out of the i-Lung, as well as those which remain trapped within its structure. The testing procedure is described in Section 2.2.2.

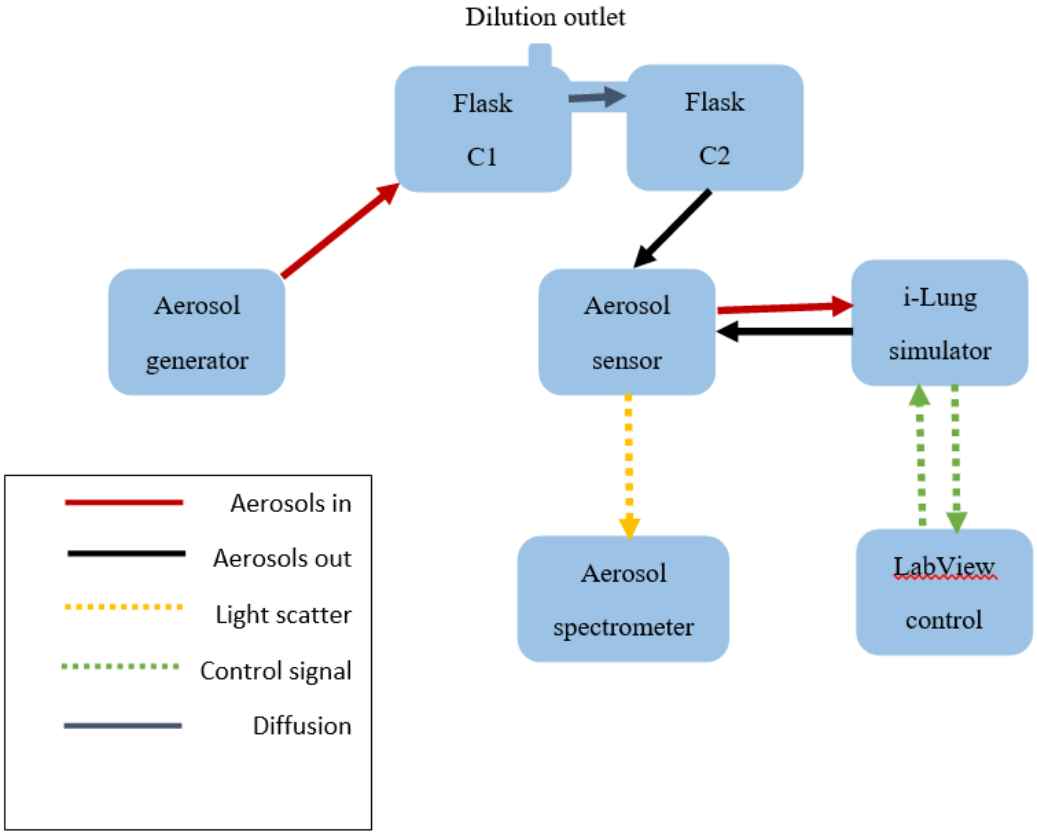

Figure 2.3: Block diagram of the experimental setup used for particle flow and deposition analysis

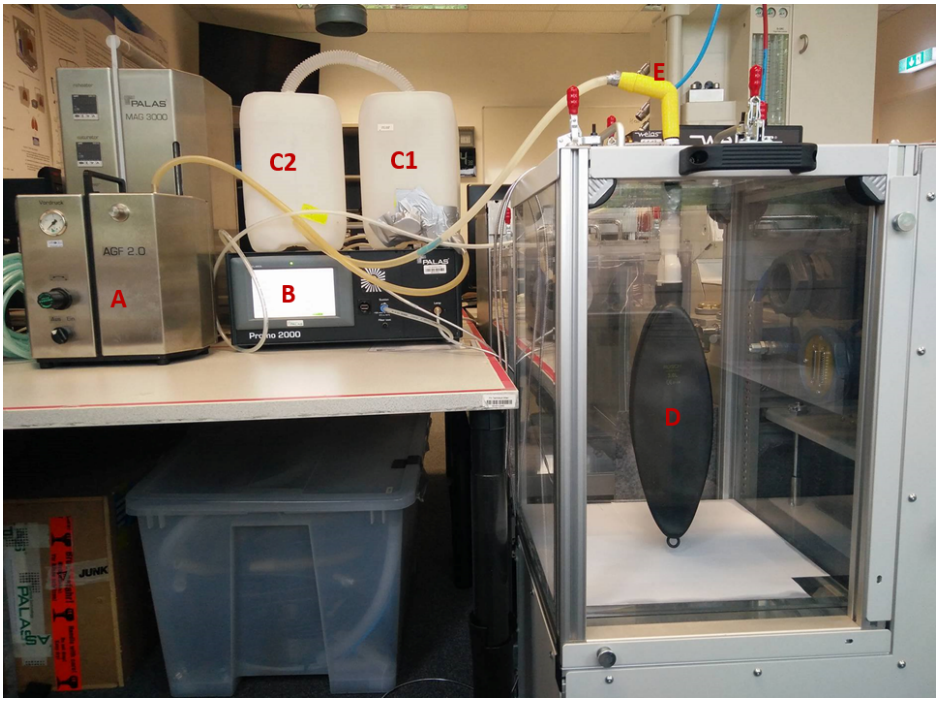

Figure 2.4: Setup for aerosol particle analysis. Aerosol generator (A); Spectrometer (B); aerosol dilution flasks (C1,C2); i-Lung (D); pharynx model (E).

Including the dilution chambers (C1, C2) was necessary in order to minimize the coincidence level (i.e. percentage of superposition of particles during the measurement) in the measurements. In particular, the aerosol generator is directly connected to the C1 chamber, allowing therefore the aerosol particles to mix with a closed volume of air. Subsequently the mixed particles travel from chamber C1 to chamber C2, through a a wide connection tube situated on the top of the chambers. At last, the mixed particles are extracted from the C2 chamber and inhaled by the i-Lung.

2.2.2 Testing procedure

The i-Lung is operated by the software LabVIEW under the conditions presented in Table 2.2. The operation window with the indicated parameters is presented in Figure 2.5.

Parameter	Value
amplitude	1.5 rps
frequency	0.2 Hz
tidal volume	0.5 L

Table 2.2: LabVIEW operation parameters for i-Lung emulating tidal breathing.

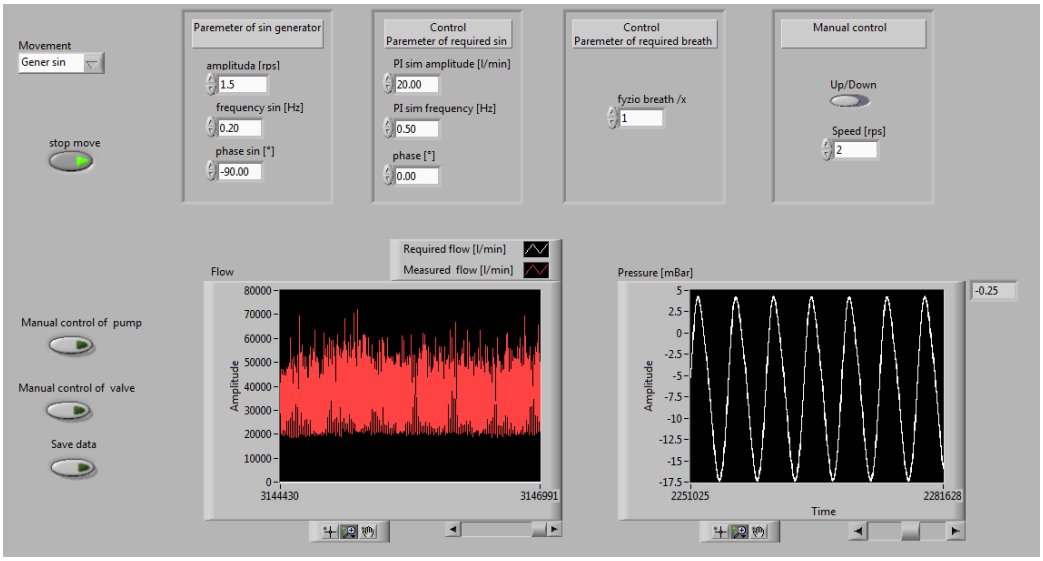

Figure 2.5: Operational window of the LabVIEW interface. The input parameters presented enable the tidal breathing mode of the i-Lung. The red oscillations on the left represent the flow; the plot on the right shows the pressure oscillations over time during tidal breathing.

The testing procedure for obtaining the results described in the Section 3, were the following:

1. Set the pressure of the aerosol generator (0.2 *bar* or 0.4 *bar*);
2. On the screen of the spectrometer a plot of number of particles over concentration will appear. Allow the function to stabilize for 120 *s*;
3. Register the time and the values obtained for the next 60 *s*;
4. Import the data into the PDAnalyze software and elaborate the data in the pre-selected range of 60 *s*.

2.2.3 Aerosol production

For the process of aerosol production, the AGF 2.0 Palas GmbH was used. The generator produces an aerosol consisting of droplets with a mean particle diameter of 0.25 μm and a maximal diameter of 10.00 μm. [25] These values are suitable for lung simulation because the size is appropriate for entering the furthest airways in the lung system. The system has an adjustable binary nozzle that enables the adjustment of the massflow.

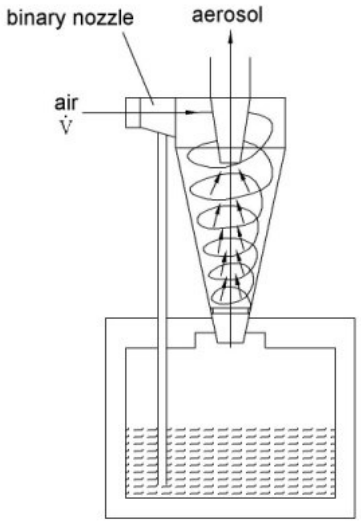

Figure 2.6: Operation principle of the AGF 2.0 aerosol generator. Taken from [26]

The aerosol source material is DEHS (Di-2-Ethylhexyl-Sebacat). Being an oil, it is not hygroscopic and therefore the application in models with high humidity values is possible. The DEHS aerosol is ejected from the generator with a maximal mass flow rate of 4 g/h. An additional dry-air inlet had to be introduced in order to diminish the aerosol concentration and not exceed the measuring range of the sensor. Moreover, this additional airflow ensures a constant aerosol transport. [25]

2.2.4 Optical spectrometer

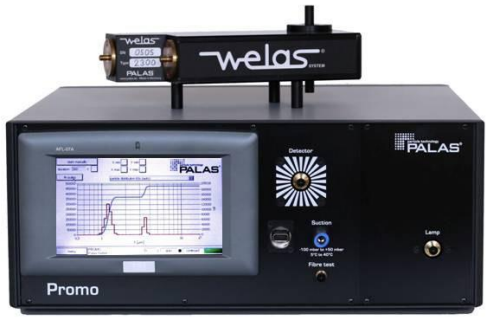

Figure 2.7: Optical aerosol spectrometer by PALAS complete with the WELAS 2070 sensor. Taken from [27]

The optical aerosol spectrometers Promo 2000 by PALAS with the sensor WELAS 2070, was used for the identification of aerosol particles. [27, 28] The welas digital system measures the scattered light intensity of poly-disperse particles. The determination of particle size happens via classification of the scattered light signal to 50 a defined calibration curve of particle diameter sections. The arrangement of measured particle sizes is separated into different size segments and a histogram is generated. The poly-disperse particles pass the measuring volume in the sensor system. Through the glass fibre cables the white light illuminates the volume and on the other side takes the detected signals for further processing to the Promo 2000 system. By the patented T aperture the measurement accuracy is improved in terms of border zone detection.[28]

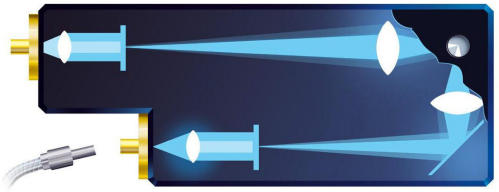

Figure 2.8: Representation of the optical measuring system (inside the sensor), with two glass fiber connectors, the patented T aperture, lenses and the passing through measuring volume. Taken from [28]

Palas parameters

Parameter	Value
Density	1000 kg/m^3
Form factor	1
Flow velocity	5 m/s
PM amplification	1.448 V
Dilution	1

Table 2.3: Palas operational parameters for aerosol flow analysis. These values can be selected on the spectrometer itself, before starting the measurement.

2.2.5 Spirometry

To ensure that the i-Lung performs tidal breathing correctly, a spirometry study was conducted. The tools used were the FlowMeter 30-D spirometer, coupled with the ThorSoft software. More specifically, the i-Lung was operated with the parameters described in Section 2.2.2, and a vital capacity (VC) study was conducted. An inevitable drift in the spirometry measurement had to be taken into account, hence the obtained data was filtered with a low-pass filter using Matlab and a curve with no pendency was obtained, as described in Section 3.2.4.

Parameter	Value
Precision	3%
Resolution	8 mL/s
Flow range	18 L/s
Digital sampling rate	100 MHz
Flow dimensions	30 mm x 150 mm
Device dimensions	27 mm x 60 mm x 150 mm
Communication	USB
Power supply	USB 5V

Table 2.4: FlowMeter 30-D product specifications. [22]

Chapter 3

Results

Following the methods described in Chapter 2, results of the numerical and experimental study were obtained. The numerical analysis presents CAD models of the airways (human and i-Lung based), and a subsequent CFD analysis of particle speed and flow direction from which particle deposition can be concluded. Furthermore, the outcome of the experimental aerosol flow and deposition analysis is portrayed.

3.1 Numerical Analysis

At first, a simplified model of the human trachea and right bronchi was designed. Subsequently, a complete airway model based on the i-Lung's airway module was designed and studied.

3.1.1 Realistic human airway model

Using Autodesk Inventor 2016, a realistic model of the trachea, bronchi and right bronchioli was designed. The geometry of the model is based on dimensions presented in literature 2.1.1, no mucus lining was included. To ensure a precise analysis, despite the simplifications already induced through the elimination of the mucus lining, a meshing size of 0.1 was intruduced based on a tetrahedron shape. The meshing time of the entire volume comprised several hours.

Figure 3.1: Airway representation of the trachea, bronchi and right bronchioli. The surface was are smooth (i.e. mucus layer has been neglected in the modeling phase). The model was realized with Autodesk Inventor 2016 and imported in FreeCAD for meshing. Meticulous tetrahedral mesh (0.1 size) indicates the complexity of the irregular structure, leading to a computational time of several hours.

3.1.2 i-Lung based airway model

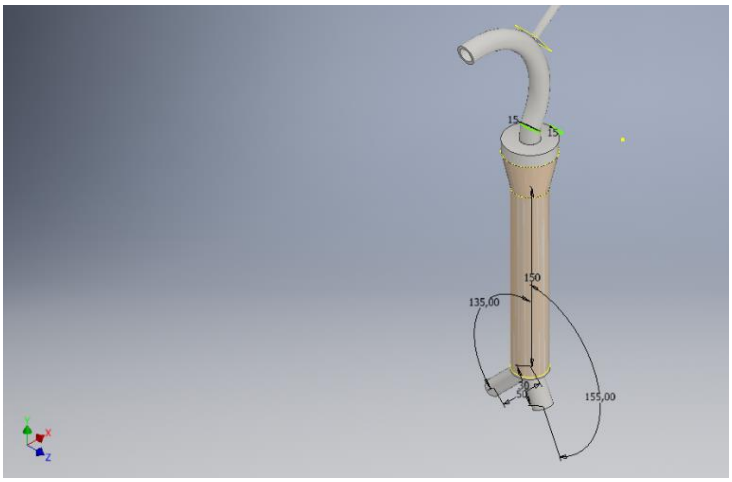

Figure 3.2: CAD model, designed with Autodesk Inventor 2016, of the laryinx, pharynx, trahcea and branching bronchi of the i-Lung. The elongated external tube represents the connection to the particle detection machine.

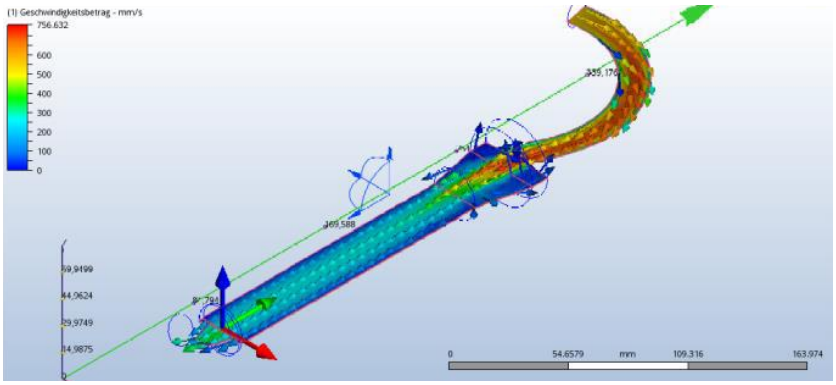

Figure 3.3: CFD simulation, using Autodesk CFD 2017, of airflow through the i-Lung based airways. The red areas, found at the narrowing of the tube, indicate the ones where the velocity of particles is the highest (756 mm/s). In the blue areas the flow is laminar. The slowest particle velocity can be identified along the internal walls of the trachea (dark blue).

3.1.3 i-Lung based pharynx model

Figure 3.4: CAD model generated with Autodesk Inventor 2016, of the inhalation duct (i.e. i-Lung based pharynx). A small hole at the bending spot will serve as a connector of the i-Lung to the spectrometer for aerosol measurement.

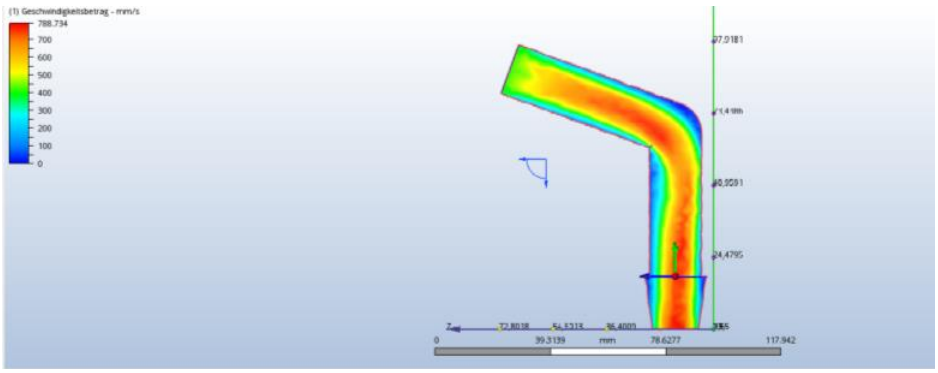

Figure 3.5: Airflow simulation, modeled in CFD Autodesk 2017, withing the connector duct (i.e. i-Lung based pharynx model). Red areas, at the curvatures and narrowing of the diameter, indicate the areas where particle velocity is at its highest (788 mm/s). Blue areas indicate locations of slow particle flow.

Figure 3.6: Printed pharynx model (yellow); support structure (gray) used solely for positioning purposes.

3.2 Experimental validation

The results presented show specifics about the aerosol flow withing the i-Lung. Concentration of aerosols, mean particle size and particle number during inhalation versus exhalation were analyzed.

3.2.1 Particle number and concentration during tidal breathing

The aerosol flow analysis data was processed by the PDAnalyze software with the aim of investigating on the quantity and concentration of particles during tidal breathing of the i-Lung. The data was observed over a time frame of 60 s. The i-Lung was operating mimicking a human tidal breathing pattern. Hence, the volume per breath was 0.5 L. These alterations of the experiment were conducted:

- $Version1$: Breathing frequency of 0.2 Hz (i.e. 12 breaths/minute) and aerosols generated at 0.2 bar pressure. The result of such conditions is a breathing pattern that oscillates between 2500 and 1500 P/s, and whose concentration oscillates between 40'000 and 15'000 P/cm^3. See Figure 3.7;
- $Version2$: Breathing frequency of 0.2 Hz (i.e. 12 breaths/minute) and aerosols generated at 0.4 bar pressure. The result of such conditions is

a breathing pattern that oscillates between 19'000 and 14'000 P/s, and whose concentration oscillates between 640'000 and 450'000 P/cm^3. See Figure 3.8;

- $Version3$: Breathing frequency of 0.5 Hz (i.e. 30 breaths/minute) and aerosols generated at 0.2 bar pressure. The result of such conditions is a breathing pattern that oscillates between 14'000 and 16'000 P/s, and whose concentration oscillates between 640'000 and 545'000 P/cm^3. See Figure 3.9.

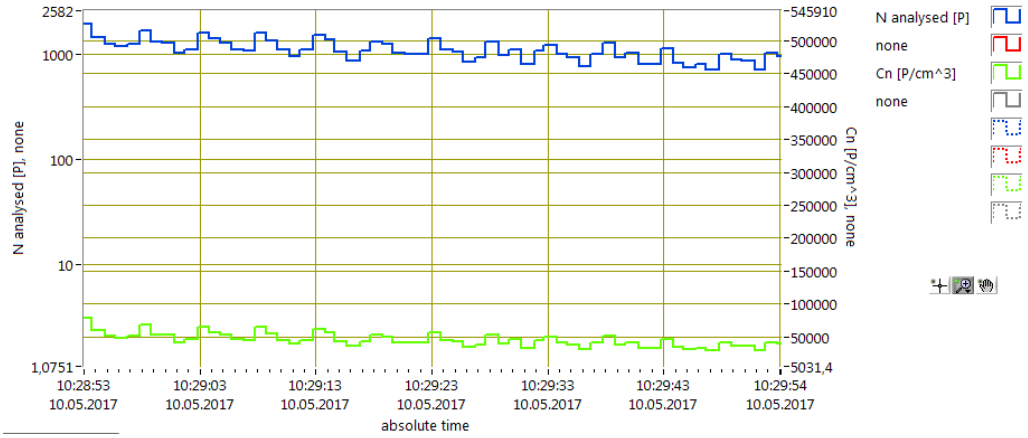

Figure 3.7: Aerosol flow analysis within the i-Lung. The blue curve represents the oscillation of the number of analyzed particles over time (60 s). The green curve represents the oscillation of the concentration $[P/cm^3]$ over time. Test parameters: tidal volume of 0.5 L ; inlet aerosol pressure of 0.2 bar; breathing frequency of 0.2 Hz.

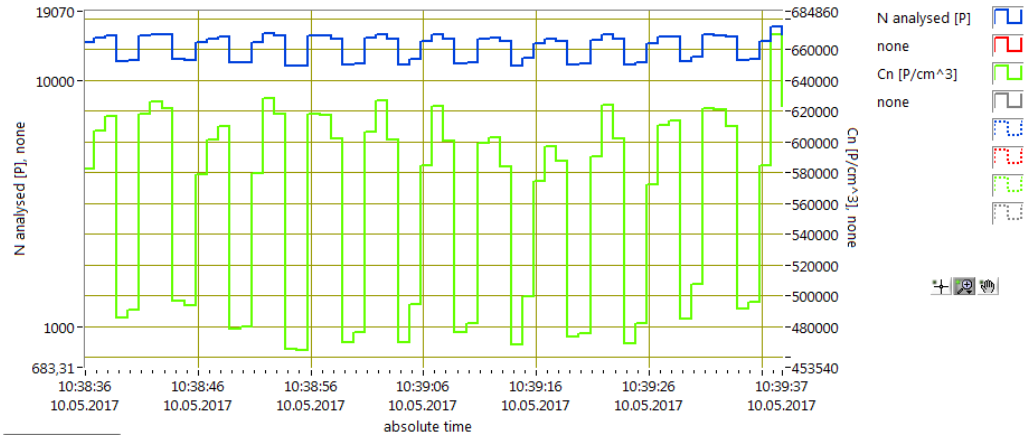

Figure 3.8: Aerosol flow analysis within the i-Lung. The blue curve represents the oscillation of the number of analyzed particles over time (60 s). The green curve represents the oscillation of the concentration [P/cm^3] over time. Test parameters: tidal volume of 0.5 L ; inlet aerosol pressure of 0.4 bar; breathing frequency of 0.2 Hz.

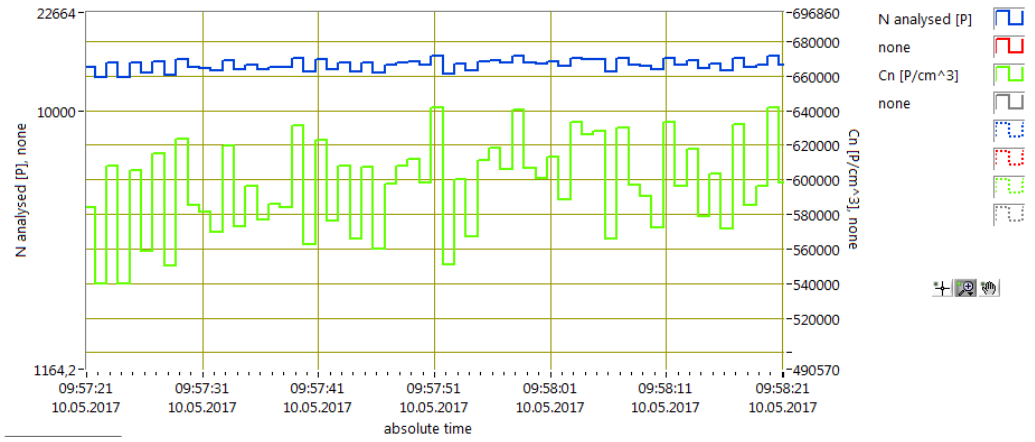

Figure 3.9: Aerosol flow analysis within the i-Lung. The blue curve represents the oscillation of the number of analyzed particles over time (60 s). The green curve represents the oscillation of the concentration [P/cm^3] over time. Test parameters: tidal volume of 0.5 L ; inlet aerosol pressure of 0.4 bar; breathing frequency of 0.5 Hz.

3.2.2 Statistical distribution of particle size

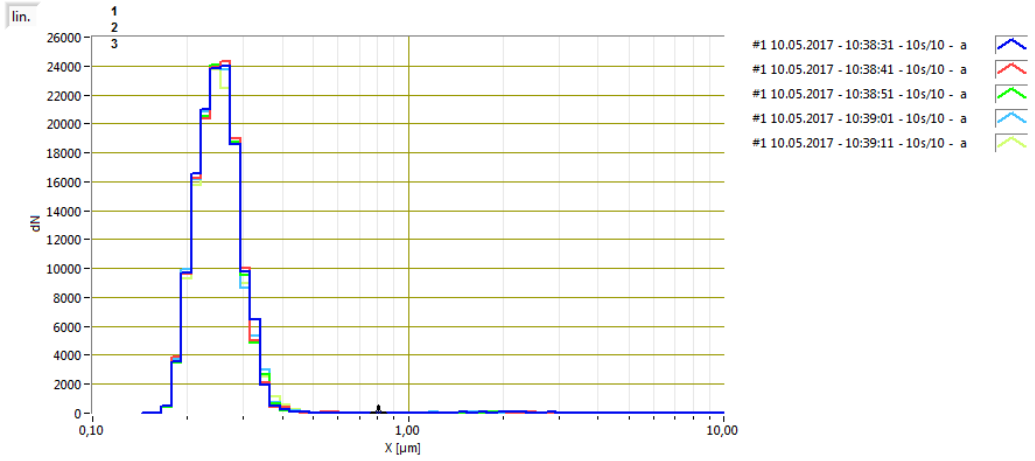

Figure 3.10: Statistical distribution of particle size during the operation of the i-Lung. Five intervals (dark blue, red, green, light blue and yellow) of 10 s each were compared. The mean of the distribution is located at 0.25 μm.

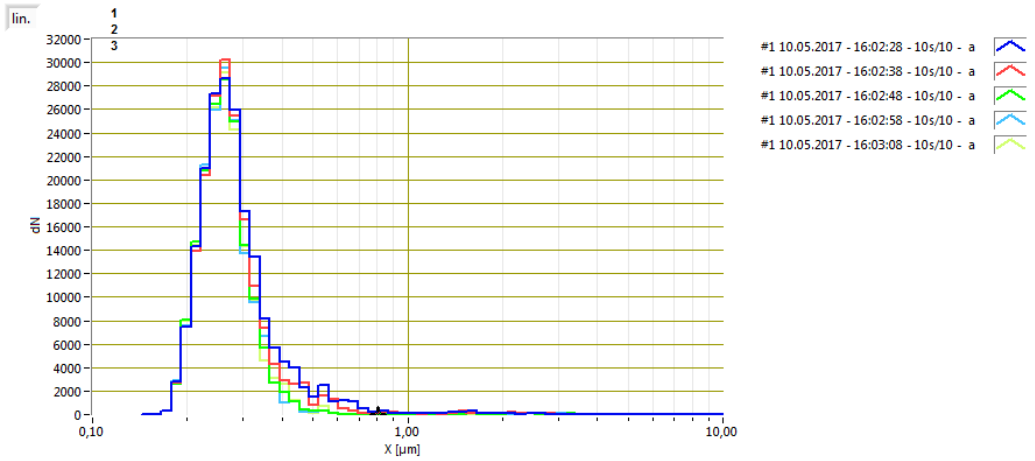

Figure 3.11: Statistical distribution of particle size during the operation of test structure. Five intervals (dark blue, red, green, light blue and yellow) of 10 s each were compared. The mean of the distribution is located at 0.26 μm.

3.2.3 Statistical distribution of particle size during inhalation and exhalation

The data presented in Figure 3.12 and Figure 3.13 shows the distribution of particle size over time during tidal breathing (i.e. 1 L/breath) of the i-Lung module. Each figure represents the overlapping of five intervals, each lasting 10 s.
A clear difference between inhalation and exhalation can be noted in the maximum values of the curves. Indeed, the inhalation maximum average corresponds to 1350 particles, on the other hand the maximum average value during exhalation is 1250 particles. Thus, the amount of particles deposited within the i-Lung module during tidal breathing is 100 particles, according to the formula:

$$d = i - e \tag{3.1}$$

where d stands for deposited particles, i stands for the amount of inhaled particles and e represents the quantity of exhaled particles.

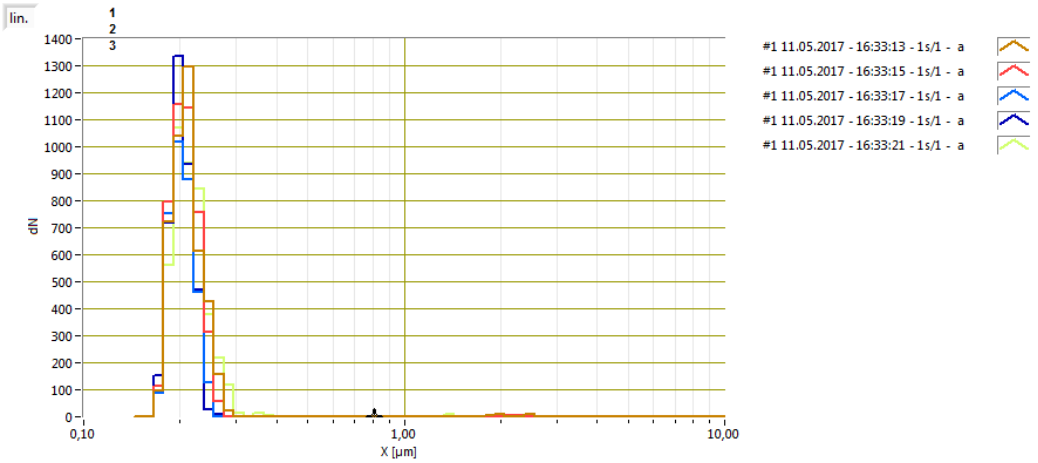

Figure 3.12: Statistical distribution of particle size during inhalation. Five intervals (brown, red, light blue, dark blue and yellow) of 1 s each were compared. The mean of the distribution is located at 0.26 μm. It can be observed that the maximum number of inhaled particles is 1350.

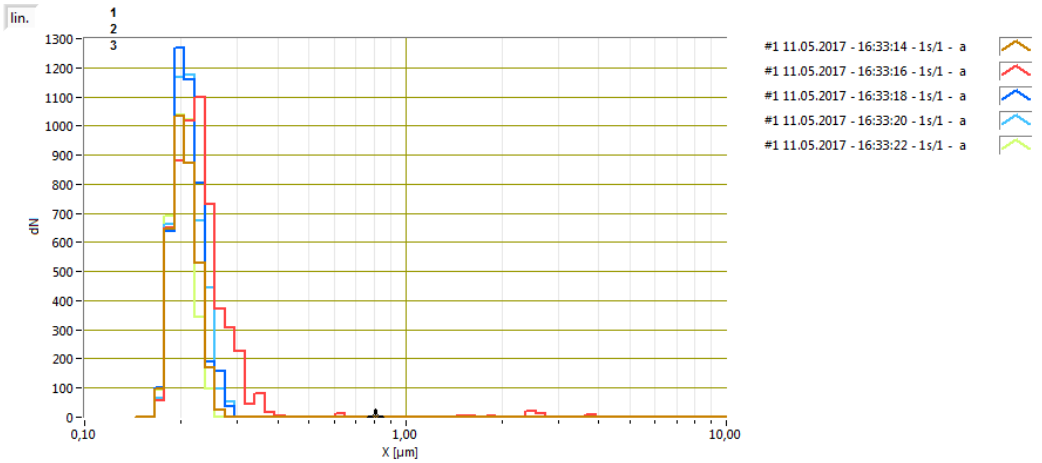

Figure 3.13: Statistical distribution of particle size during exhalation. Five intervals (brown, red, blue, green and yellow) of 1 s each were compared. The mean of the distribution is located at 0.26 μm. It can be observed that the maximum number of exhaled particles is 1250.

3.2.4 i-Lung spirometry data

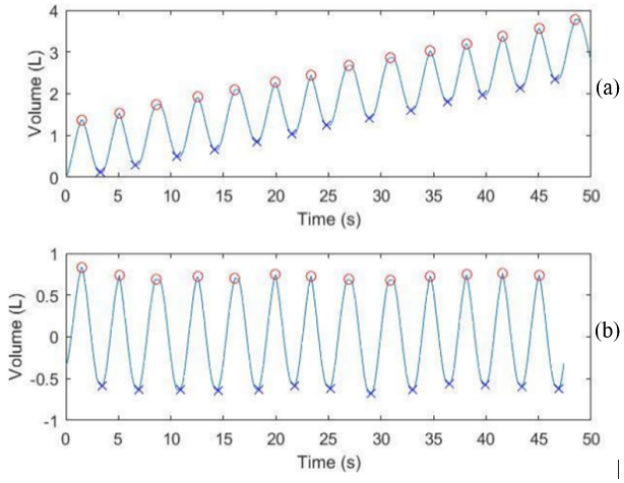

Figure 3.14: Spirometry data from tidal breathing pattern of the i-Lung. (a) shows the raw data collected with the FlowMeter 30-D spirometer, a drift is noticeable; (b) presents the result of low-pass filtering the low data; no drift appears.

Chapter 4

Discussion

The results presented in Chapter 3 are justified and conclusions are drawn from both, numerical and experimental study. Differences in the numerical model of human airways and i-Lung based trachea and bronchi are highlighted Furthermore, the results of the experimental validation are compared to literature values.
Improvements of the numerical model as well as the experimental setup are suggested in Section 4.4.

4.1 Numerical Analysis

The drawbacks of a numerical simplified model of the human airways are highlighted and alternatives are presented. Subsequently, conclusions about the particle flow path within the i-Lung airways is discussed, along with suppositions about the deposition quantity and location of the aerosol particles.

4.1.1 Realistic human airway model

In order to perform a valuable and reliable simulation of airflow within the human respiratory tract, it is necessary to rely on CT geometry. Reason for this is that small changes in geometry can have a strong impact on the flow of particles within the duct. Hence, designing a simplified model of the trachea, bronchi and bronchiole leads to results that are unsuitable for a comparison to reality as well as an experimental model. See Section 1.6 and

Section 3.
Figure 3.1 shows a CAD model of realistic human airways. The model presents a full structure only for the right bronchi, because of the complexity of the model. Indeed, it has been found that the meshing time by far exceeds an accepted limit, and therefore renders the model unsuitable for for a CFD analysis. Initially, the right bronchioli was chosen for the modelling because previous research supports the belief that it has a greater influence on the airflow distribution. See Section 1.6.

4.1.2 i-Lung based airway model

Figure 3.2 shows the CAD model that has been designed to represent the i-Lung based airways. The CFD analysis that has been based on it, shows results presented in Figure 3.3. It has been proven that the narrowing of the ducts causes the velocity of the particles to increase, as well as that the particles tend to flow through the right bronchi. Indeed, more particles flow through the right bronchi and into the right lung lobe because the angle of inclination is smaller (c.a. 25 °) compared to the left one (c.a. 45 °). This is due to the fact that the heart is located slightly to the left within the chest. This increase in bifurcation angle causes a higher disruption of the flow of particles through the trachea and therefore leads to a smaller number of particles landing in the left lung lobe. Furthermore, the right bronchi is shorter in length due to the compression of the liver beneath but therefore wider in diameter compared to the left bronchi. Therefore it can also be concluded that more particles deposit in the left lobe; given its greater angle the particles are less likely to be ejected during exhalation.
Furthermore, the locations where change of diameter occurs (e.g. from larynx to trachea) were characterized by turbulent flow, whereas areas with a constant diameter (e.g. along the trachea) presented laminar flow.

4.2 Experimental validation

Results have shown that the experimental setup for the measuring of particle flow and deposition was suitable. Nevertheless, in order to further improve the precision of the outcome a mono-disperse generator should be operated instead of a poly-disperse one. Reason for this is the fact that by having a poly-disperse generator the particles analyzed are of different sizes. Instead,

by having a mono-disperse generator it would be possible to monitor the exact quantities of particles of specific size, for both: flow rate and deposition.

4.2.1 Oscillation of particle number and concentration during tidal breathing

Figure 3.7 shows that a pressure of 0.2 bar for the aerosol generation is too low. Indeed, the pattern of inhalation and exhalation of the i-Lung can be observed, both in the particle number function as well as in the concentration function. Nevertheless, the differences in concentration and particle number are not highlighted.
Figure 3.8 shows that by increasing the aerosol generation pressure up to 0.4 bar, the pattern of inhalation and exhalation is very clear. Indeed, the curve representing the particle number oscillates within a definite range, underlining the difference of particles being inhaled and exhaled. On the other hand, the concentration curve clearly follows the pattern of the particle number curve. A clear oscillation in concentration quantity can be identified between inhalation and exhalation.
Figure 3.9 shows that by increasing the breathing frequency to 0.5 Hz (i.e. 30 breaths/minute), the particle number curve is no longer synchronized with the concentration curve. This may be due to the fact that with a high breathing frequency, the particle concentration changes swiftly within the lungs, yet within the spectrometer the particles collide. Indeed, in this experiment a high coincidence percentage has been observed, therefore confirming the hypothesis that the particle number function is too slow to adapt to elevated changes in concentration. However, this experiment had a solely observational purpose. Being the breathing frequency during tidal breathing 0.2 HZ, which is an equivalent to 12 breaths/minute, the inability of the quantity function to follow the concentration function does not have repercussions on the definition of reliability of the testing structure. In fact, previous experiments that have been conducted on the basis of real-life parameters were successful.

4.2.2 Statistical distribution of particle size

Figure 3.10 indicates that the mean particle diameter observed during the aerosol flow through the i-Lung, is 0.25 μm. In order to test the veridicity of this result, the analysis has been conducted in an open loop, hence without the intervening of the i-Lung. The results of the outcome of the analysis of aerosol flow through the test structure are presented in Figure 3.11. The latter shows that the mean diameter of the particles is slightly bigger, in particular is measures 0.26 μm. This small shift in value can be given by the fact that some larger particles remain trapped within the i-Lung, whereas they continue their flow in the setup where the i-Lung is not present. Furthermore, by removing the i-Lung from the setup, the probability that the particles will sedimentate is reduced due to the fact that the i-Lung itself generates a alteration in flow, during inhalation and exhalation.
Nevertheless, this change in mean diameter is negligible and the testing structure can therefore be considered a valid setup.

4.2.3 Statistical distribution of inhaled and exhaled particles

Figure 3.12 presents a statistical distribution of particle size during inhalation. The maximum number of inhaled particles in a cycle lasting 1 s comprises c.a. 1350 particles. On the other hand, Figure 3.13 presents a statistical distribution of particle size during exhalation. The maximum number of exhaled particles in a cycle lasting 1 s is c.a. 1250 particles. It can therefore be concluded that 100 particles (i.e. inhalation - exhalation = 1350 - 1250), remain trapped in the i-Lung and the adjacent tubing structure. It must however be considered that the i-Lung does not have an internal structure of bronchioli within its latex-lung lobes, and therefore is a simplified representation of reality. Indeed, as presented in Section 1.6, a high number of particles remains trapped in the bifurcations of the vasculature within the lung lobes. On the other hand, the human airway duct has structures such as cilia along its internal walls, that prevent particles from depositing and sedimenting permanently. Indeed, large particles trapped within the trachea and bronchi are transported back upwards by these hair-like structures, where they are subsequently exhaled from the mouth. The i-Lung model is not capable of performing such a

complex elimination process, therefore the particles that can not be ejected during exhalation sediment along its internal walls.
A further improvement would be the inclusion of an open system, in order to create a continuous flow of aerosols. The system currently used is a closed one, the aerosols particles dilute with air only in closed flasks (C1, C2),(Figure 2.3). By introducing an open systems, the aerosols would not accumulate and increase in concentration within the flasks. This would result in a more equally distributed concentration of aerosols over time.

4.2.4 i-Lung spirometry data

Figure 3.14 presents the tidal breathing pattern performed by the i-Lung during a vital capacity test. The spirometry results had to be filtered in order to remove a gradual drift, which is given by an unknown internal error of the spirometer itself and not by a lack of performance of the i-Lung. The plot shows that the i-Lung is capable of emulating tidal breathing reliably, indeed the alternations of inhaled and exhaled volumes are symmetrical and correspond to the volumes exchanged by human lungs (i.e. 0.5 L per inhalation and per exhalation). It can therefore be concluded that the i-Lung has a reliable performance for a study concerned about particle flow and deposition.

4.3 Conclusion

With the aim of investigating the aerosol particle flow and deposition within a lung simulator, the i-Lung, two approaches have been introduced. On the one hand, a numerical analysis has been conducted, providing information about particle velocity and critical deposition areas within the i-Lung airways. On the other hand, an experimental approach has led to results that enable to draw conclusions on particle number, concentration and dimensions during tidal breathing. It appears that the setup used for the study, consisting primarily of a liquid aerosol generator, dilution flasks, a spectrometer and the i-Lung leads to plausible results. To confirm the reliability of the i-Lung simulator, a spirometry study has been conducted and the tidal breathing volume has been categorized as correspondent to human tidal volumes.
Particle flow analysis has shown that the aerosol concentration, along with

the particle number, is tightly bound to the breathing pattern. Furthermore, by analyzing the number of particles being inhaled and the ones being exhaled by the i-Lung machine, it was possible to identify the quantity of particles that deposit within the system.
Comparing the results of both, numerical analysis and experimental validation to literature, the validity of both models was confirmed. Indeed, particles of 0.25 μm size are the ones that deposit the least within an airway system. Moreover, comparing amounts of inhaled versus exhaled particles of a tidal breathing pattern, it was shown that a minor fraction of aerosols remain trapped within the airways. This is partially due to the fact that particles tend to adhere to internal linings of tubing when there is a change of geometry and diameter (e.g. pharynx to larynx) and partially due to the fact that the i-Lung, unlike real human airways, does not present a cilia-lining structure that could move the trapped particles back to the mouth opening for them to be exhaled.

4.4 Outlook

Further steps consist in conducting further CFD analysis of the i-Lung trachea model and the connector duct, in order to define particle deposition depending on the size. In order to obtain validation for this numerical evaluation, an experimental study has to be conducted. The setup designed for this study will be viable also for a size-specific particle deposition study, however the aerosol poly-disperse generator should be substituted with a mono-disperse generator. This will ensure a valid monitoring of alterations in the quantity of particles entering and exiting the i-Lung, as their size will be homogeneous.
Furthermore, testing can be extended by substituting the latex-lung lobes with a primed porcine lung. The tests can be conducted following the same procedure. An advantage of this study would be the identification of the influence of an internal structure (i.e. bronchioli and alveoli) on particle deposition and particle flow. Moreover, a truly realistic study would be the replacement of the primed porcine lung with a fresh porcine lung. Justification for this study would be the fact that by priming the respiratory organ, the alveoli tend to agglomerate and collapse on themselves. Therefore, the surface area involved in the gas exchange is smaller in a primed organ compared to the one of a fresh organ.

Bibliography

[1] European parliament. Directive 2010/63/eu of the european parliament and the council on the protection of animals used for scientific purposes. *EU Official Journal*, 2010.

[2] Burch R.L. Russell W.M. The principles of humane experimental technique. *Methuen*, 1959.

[3] Devolder T. et al. Research expenditure for 3r alternatives a review of national public funding programmes in european countries. *ALTEX*, 2014.

[4] Ask B. Buzek J. Regulation (ec) no 1223/2009 of the european parliament and of the council of 30 november 2009 on cosmetic products. *Official Journal of the European Union L 342*, 2009.

[5] Myers T. Ari A., Hess D. and Rau J. A guide to aerosol delivery devices for respiratory therapists. 2nd ed. *American Association for Respiratory Care*, 2009.

[6] Baron P.A. and K. Willeke. Aerosol measurement: Principles, techniques, and applications, 3rd edition. *A Wiley Interscience Publication John Wiley and Sons, Inc.*, 2011.

[7] West J.B. Pulmonary pathophysiology - the essentials. 7th ed. *Lippincott Williams and Wilkins.*, 2005.

[8] Darquenne C. Particle deposition in the lung. *Encyclopedia of Respiratory Medicine*, 2006.

[9] Wanger et al. Standardisation of lung function testing standardisation of the measurement of lung volumes. *Revue des Maladies Respiratoires 24.3*, 2007.

[10] Fourth edition International labour office. *Enciclopedia of Occupational Health and Safety, Chapter 10: Respiratory System*, Accessed on 12/05/2017). Available at: `http://www.ilocis.org/documents/chpt10e.htm`.

[11] Palas Gmbh. Practical basic knowledge regarding aerosol technology. *1st edistion*, 2008.

[12] J. Schneider. Physik und chemie des athmosphaerischen aerosols. *Max-Planck-Institut fuer Chemie, Mainz*, 2006.

[13] Hinds W.C. Properties, behavior and measurement of airborne particles, second edition. *A Wiley Interscience Publication John Wiley and Sons, Inc.*, 1999.

[14] Moelter L. Helsper C. Erzeugung von pruefaerosolen fr die kalibrierung von optischen partikelmessverfahren nach vdi 3491. *Technisches Messen 56:229- 234.*, 1989.

[15] K. Stiglbrunner. Aerosol measurement technologies for respiratory research purposes. *Master thesis, FH Technikum Wien.*, 2011.

[16] Vidyasagar L. DeLouise E. Physicochemical factors that affect metal and metal oxide nanoparticle passage across epithelial barriers. *Wiley Interdisciplinary Reviews: Nanomedicine and Nanobiotechnology Vol 1 Nr 4 Pages 434-450*, 2009.

[17] *Anatomy of lung segments*, accessed on 25/07/2016. Available at: `http://anatomy-bodychart.us/tag/normal-ct-anatomy-of-lung-segments/`.

[18] Andrew R. et al. Lambert. Regional deposition of particles in an image based airway model: large eddy simulation and left-right lung ventilation asymmetry. *Aerosol Science and Technology 45.1*, 2011.

[19] Sauret Islam M. S., Saha S.C. Numerical investigation of aerosol particle transport and deposition in realistic lung airway. *Queensland University of Technology Australia*, 2015.

[20] Wurm M. Entwicklung eines aktiven lungenmodells. *Msc Thesis, FH Technikum Wien*, 2010.

[21] RWETC S.R. Lung model 2.1 simulator, documentation revision 1.1. *College of Polytechnics Jihlava*, 2014.

[22] Agojo S. Milanovic S., Krizanac M. Development of a set of respiration values and comparison to a porcine lung simulator. *University of Applied Sciences Technikum Wien*, June 2016.

[23] G. Cumming. Horsfield K. Angles of branching and diameters of branches in the human bronchial tree. *Bulletin of Mathematical Biology 29.2: 245-259*, 1967.

[24] Intechopen. *Trachea dimensioning*, Accessed on 24/07/2016). Available at: `http://www.intechopen.com/source/html/18257/media/image4.jpeg`.

[25] Available at:. *Palas GmbH. Aerosolgeneratoren Serie AGF*, Accessed on 25/01/2016. `http://www.allfield.com.tw/sites/default/files/attachments/AGF.pdf`.

[26] Palas Gmbh. Aerosol generator series agf 2.0. *Specification user manual for measurements*, 2017.

[27] Palas Gmbh. Produktdatenblatt: Die welas sensoren fuer das welas digital system und promo. *Karlsruhe*, 2010.

[28] Palas Gmbh. Schulung partikelmesstechnik: Funktion streulichtspektrometersystem welas digital. *Karlsruhe*, 2010.

List of Figures

List of Tables